The Atmospheric Carbon and Transport (ACT) – America Mission

Kenneth J. Davis,[a, b], Edward V. Browell,[c] Sha Feng,[a, d] Thomas Lauvaux,[e] Michael D. Obland,[f] Sandip Pal,[g] Bianca C. Baier,[h, i] David F. Baker,[j] Ian T. Baker,[j] Zachary R. Barkley,[a] Kevin W. Bowman,[k] Yu Yan Cui,[a] A. Scott Denning,[l] Joshua P. DiGangi,[f] Jeremy T. Dobler,[m] Alan Fried,[n] Tobias Gerken,[a, o] Klaus Keller,[p, b] Bing Lin,[f] Amin R. Nehrir,[f] Caroline P. Normile,[a, q] Christopher W. O'Dell,[j] Lesley E. Ott,[r] Anke Roiger,[s] Andrew E. Schuh,[j] Colm Sweeney,[i] Yaxing Wei,[t] Brad Weir,[u, r] Ming Xue,[v] and Christopher A. Williams[w]

[a] *Department of Meteorology and Atmospheric Science, The Pennsylvania State University, University Park, PA*

[b] *Earth and Environmental Systems Institute, The Pennsylvania State University, University Park, PA*

[c] *STARSS-III Affiliate, NASA Langley Research Center, Hampton, VA*

[d] *now at Atmospheric Sciences and Global Change Division, Pacific Northwest National Laboratory, Richland, WA*

[e] *Laboratoire des sciences du climat et de l'environnement, Université Paris-Saclay, CNRS, CEA, UVSQ CEA-Saclay, l'Orme des Merisiers, Gif-sur-Yvette, France*

[f] *NASA Langley Research Center, Hampton, VA*

[g] *Atmospheric Science Division, Texas Tech University, Lubbock, TX*

[h] *Cooperative Institute for Research in Environmental Sciences, University of Colorado, Boulder, CO*

[i] *NOAA Global Monitoring Laboratory, Boulder, CO*

[j] *Cooperative Institute for Research in the Atmosphere, Colorado State University, Fort Collins, CO*

[k] *Jet Propulsion Laboratory, California Institute of Technology, Pasadena, CA*

[l] *Department of Atmospheric Science, Colorado State University, Fort Collins, CO*

[m] *Spectral Sensor Solutions LLC, Fort Wayne, IN*

[n] *Institute of Arctic and Alpine Research, University of Colorado, Boulder, CO*

[o] *now at School of Integrated Sciences, James Madison University, Harrisonburg, VA*

[p] *Department of Geosciences, The Pennsylvania State University, University Park, PA*

[q] *now at the Bipartisan Policy Center, Washington, D.C.*

[r] *NASA Goddard Space Flight Center, Greenbelt, MD*

[s] *Deutsches Zentrum für Luft- und Raumfahrt (DLR), Institut für Physik der Atmosphäre, Oberpfaffenhofen, Germany*

[t] *Environmental Sciences Division, Oak Ridge National Laboratory, Oak Ridge, TN*

[u] *Universities Space Research Association, Columbia, MD*

[v] *Center for Analysis and Prediction of Storms and School of Meteorology, University of Oklahoma, Norman OK*

[w] *Graduate School of Geography, Clark University, Worcester, MA*

Corresponding author: Kenneth J. Davis, kjd10@psu.edu

ABSTRACT

The Atmospheric Carbon and Transport (ACT) – America NASA Earth Venture Suborbital Mission set out to improve regional atmospheric greenhouse gas (GHG) inversions by exploring the intersection of the strong GHG fluxes and vigorous atmospheric transport that occurs within the midlatitudes. Two research aircraft instrumented with remote and in situ sensors to measure GHG mole fractions, associated trace gases, and atmospheric state variables collected 1140.7 flight hours of research data, distributed across 305 individual aircraft sorties, coordinated within 121 research flight days, and spanning five, six-week seasonal flight campaigns in the central and eastern United States. Flights sampled 31 synoptic sequences, including fair weather and frontal conditions, at altitudes ranging from the atmospheric boundary layer to the upper free troposphere. The observations were complemented with global and regional GHG flux and transport model ensembles. We found that midlatitude weather systems contain large spatial gradients in GHG mole fractions, in patterns that were consistent as a function of season and altitude. We attribute these patterns to a combination of regional terrestrial fluxes and inflow from the continental boundaries. These observations, when segregated according to altitude and air mass, provide a variety of quantitative insights into the realism of regional CO_2 and CH_4 fluxes and atmospheric GHG transport realizations. The ACT-America data set and ensemble modeling methods provide benchmarks for the development of atmospheric inversion systems. As global and regional atmospheric inversions incorporate ACT-America's findings and methods, we anticipate these systems will produce increasingly accurate and precise sub-continental GHG flux estimates.

CAPSULE (BAMS ONLY)

Midlatitude weather systems contain large gradients in greenhouse gases (GHG), reflecting regional fluxes and continental inflow. ACT-America carbon weather observations provide a synoptic-scale benchmark for GHG flux and transport models.

Introduction

Unknowns in the Earth's carbon cycle. Understanding the terrestrial carbon cycle is essential for diagnosing current and predicting future climate change (Marquis and Tans, 2008; Gregory et al., 2009; Michalak *et al*., 2011). Our current understanding of the earth's carbon cycle is limited. We know global anthropogenic carbon dioxide (CO_2) emissions with good accuracy, and that the Earth's terrestrial biosphere has been a strong net sink of atmospheric (CO_2) for more than three decades (Ciais et al., 2013) slowing the accumulation of CO_2 caused by fossil fuel burning. The causes of these biogenic CO_2 sinks (Huntzinger et al, 2017), their location (Peylin *et al*. 2013; Crowell et al., 2019), and their likely evolution in the future (Friedlingstein *et al*., 2014), remain deeply uncertain, contributing considerable uncertainty to climate projections (Stocker *et al*., 2013; Friedlingstein et al., 2014, Holden et al., 2018). Terrestrial biosphere models of ecosystem-atmosphere CO_2 exchange diverge substantially in their regional simulations of gross primary productivity (GPP) and ecosystem respiration (RE), and show large differences in net ecosystem-atmosphere exchange of CO_2 (NEE) at seasonal and annual time scales (Huntzinger et al., 2012; Fisher et al, 2014; Schwalm et al., 2015).

Methane (CH_4) is accumulating in the atmosphere (Montzka *et al*., 2011, Dlugokencky *et al*., 2011) and is the second largest contributor to contemporary anthropogenic climate change (Myhre et al., 2013). Fluctuations in the global rate of increase of atmospheric CH_4 (Nisbet et al., 2014) remain unexplained (Turner et al, 2019). Anthropogenic CH_4 emissions from inventories have been shown to have large biases (e.g. Miller et al., 2013; Alvarez et al.,

2018), but these biases are not clearly related to the fluctuations (Bruhwiler et al., 2017; Lan et al., 2019). Estimates of wetland CH_4 emissions diverge by nearly a factor of two on a global scale (Saunois et al., 2016) and by more than a factor of four in North America (Bloom et al., 2017).

How can atmospheric inversions help? Atmospheric inversions have the potential to provide ongoing, accurate and precise diagnoses of CO_2 and CH_4 fluxes. Atmospheric inversions (e.g., Baker *et al*., 2006a, 2010; Peters et al., 2007; Lauvaux et al, 2012; Peylin et al., 2013; Crowell et al, 2019) combine a first guess of fluxes (e.g., a model of ecosystem respiration and photosynthesis), referred to as a prior flux estimate, with winds and vertical mixing from an atmospheric transport reanalysis. The prior fluxes are propagated through the atmospheric transport fields to predict space-time distributions of atmospheric CO_2 and CH_4 (hereafter collectively referred to as C) concentrations (hereafter we will use the more precise term of mole fraction). The simulated C mole fractions are then compared to observations, such as those collected by the Global Greenhouse Gas Reference Network (GGGRN, Conway *et al*., 1994; Dlugokencky *et al*., 2005; Andrews et al., 2014; Sweeney et al., 2015) or satellite platforms (Yokota *et al*., 2009; Kuze et al, 2016; Crisp et al, 2017; Hu et al, 2018; Eldering et al, 2019). The C flux estimates are then adjusted to minimize the difference between the observed and modeled atmospheric C mole fractions.

Challenges facing atmospheric inversions. Atmospheric inversions provide invaluable insights into global to zonal, decadal-scale sources and sinks of C (e.g., Tans *et al*., 1990; Ciais *et al*., 1995; Battle et al., 2000; Bousquet *et al*., 2006). Atmospheric inversions still struggle, however, to inform regional-scale C fluxes (Peylin et al., 2013; Crowell et al., 2019). Our limited understanding of the Earth's carbon cycle stems arguably from our limited ability to diagnose routinely earth-atmosphere fluxes at regional scales. Regional

scales are critically important because they are the scales over which changes in the environment (e.g. climate, nutrients, insects, fire) and human activity (e.g. energy systems, land use and land cover) drive changes in terrestrial C fluxes.

A growing observational network. Globally-comparable, spatially and temporally extensive and dense atmospheric C measurements are essential for inferring earth-atmosphere fluxes of C using atmospheric inversions. Relevant spatial and temporal differences in atmospheric C are small, setting stringent demands on measurement calibration (WMO, 2018). Despite these challenges, the global observational network for atmospheric C is growing, bringing the potential for greater atmospheric constraint on regional C fluxes.

The most dramatic recent increases in observations have come from satellite remote sensing, including the Greenhouse gases Observing Satellite (GOSAT, Yokota et al., 2009; Kuze et al, 2016), the Orbiting Carbon Observatory-2 and -3 (OCO-2, -3; Crisp et al, 2017; Eldering et al, 2019), the TROPOspheric Monitoring Instrument (TROPOMI; Hu et al., 2018), and the Cross-Track Infrared Sounder (CrIS; Nalli et al., 2020). GeoCarb, planned for launch in 2022, will measure CO_2, CH_4 and CO over the Americas from geostationary orbit (Moore et al., 2018; Polonsky et al., 2014). Evaluation of space-based measurements remains a significant challenge. Considerable progress has been made on this topic (O'Dell et al., 2018), but evaluation has been largely limited to single-point observations (Wunch et al., 2011; 2017). Long-term, in situ measurement networks have also expanded in recent decades, including tower-based (Andrews et al., 2014; Miles et al., 2012; Hazan et al, 2016) and airborne (Sweeney et al., 2015; Machida et al., 2008) monitoring.

Atmospheric inversion systems have been adapted to include the expanded remote and in situ observation networks, with some success at determining regional C fluxes (e.g. Hu et al., 2019; Liu et al., 2017; Schuh et al., 2013). Nevertheless, large uncertainties remain in North

American total CH_4 and biogenic CO_2 fluxes (Bruhwiler et al., 2017; USGCRP, 2018; Crowell et al., 2019). Why, given the relatively high density of observations available in North America, do large uncertainties in C fluxes persist?

Prior fluxes. Two factors beyond atmospheric observations limit the accuracy of atmospheric inversions. One is uncertainty in prior flux estimates. Atmospheric inversions are complex optimizations that can be strongly influenced, especially when atmospheric C data are limited, by their "first guess" or prior fluxes. Large biases and poorly quantified uncertainties in these prior fluxes will hinder atmospheric inverse C flux estimates.

The importance of atmospheric transport. Uncertainty in atmospheric transport is a second major source of uncertainty in inverse flux estimates (Baker *et al*., 2006b; Stephens *et al*., 2007; Gerbig *et al*., 2008; Chevallier *et al*., 2010; Lauvaux and Davis, 2014; Díaz-Isaac et al, 2018; Schuh et al., 2019). Atmospheric transport uncertainty in inverse estimates of net biogenic CO_2 fluxes for temperate North America is 0.3-0.5 PgC yr^{-1} (Gurney *et al*., 2002; Baker *et al*., 2006b; Schuh et al., 2019), nearly equal to the estimated magnitude of the net annual flux. What are the causes of this uncertainty, and what can be done to reduce it?

Improved representation of mid-latitude weather systems in atmospheric inversions is highly likely to improve the resulting inverse C flux estimates. Mid-latitude weather systems are both important drivers of the global redistribution of atmospheric C (Parazoo et al., 2008; 2011; 2012; Chan et al, 2008; Barnes et al., 2016; Schuh et al., 2019), and major drivers of regional atmospheric C patterns that carry regional C flux information (Hurwitz et al., 2004; Barkley et al., 2019a; Pal et al., 2020a; Hu et al., 2021). Mid-latitude cyclones create north-south exchange of C in the cyclonic circulation, large-scale vertical lifting at frontal boundaries, and vertical mixing via convective instability (Parazoo et al., 2008; 2011; Samaddar et al., 2021).

158 Improving the resolution of the atmospheric models used in inverse modeling systems
159 may reduce transport errors. Agusti-Panadera et al., (2019) used a global weather forecasting
160 system to show that increasing the resolution of an atmospheric transport simulation reduces
161 model-data errors in atmospheric CO_2. Regional studies with high-density in situ atmospheric
162 observation networks and regional, mesoscale atmospheric models (Lauvaux et al., 2012;
163 Schuh et al., 2013) have inferred regional biogenic CO_2 fluxes to an uncertainty level capable
164 of evaluating agricultural inventories (Ogle et al., 2015). Hu et al., (2019) showed success in
165 deriving temporal variations in North American biogenic CO_2 fluxes using a continental-scale
166 mesoscale modeling system. Regional inversion systems are still relatively rare. The
167 resolution of global inversions is increasing, and the native atmospheric transport reanalyses
168 used in these systems may already be sufficiently resolved to simulate C transport by
169 synoptic weather systems with good fidelity.

170 Data are needed to evaluate and improve the representation of weather systems in
171 atmospheric inversions. Current long-term observational systems, in situ and remote, do not
172 have sufficient spatial resolution and coverage to describe the spatial structures of C within
173 midlatitude weather systems, and thus have limited ability to evaluate atmospheric
174 simulations of C transport by weather systems.

175 *Value of an airborne mission*. ACT-America is an airborne mission working toward the
176 development of a new generation of high-resolution, weather-resolving, ensemble-based
177 atmospheric C inversion systems. This mission complements long-term, global-scale
178 observations such as those made by the NOAA Global Greenhouse Gas Reference Network
179 and the growing constellation of C satellites, and airborne campaigns such as the
180 Atmospheric Tomography Mission (AToM, Prather et al., 2018) focused on the remote
181 atmosphere. ACT-America flights fill the observational gap left among continuous-in-time

182 but spatially-sparse, tower-based C measurements (Andrews et al., 2014), spatially-extensive,
183 but spatially- and temporally-sparse long-term aircraft profiling (Sweeney et al., 2015), and
184 globally-extensive but temporally-sparse (compared to synoptic weather) provided by low-
185 earth-orbit satellite systems (Kuze et al, 2016; Crisp et al, 2017). Here we present ACT-
186 America's mission design, and an interpretation of the results emerging from the project.

187 ## Mission Goals and Objectives

188 The ACT-America mission's overarching goal is to enable atmospheric inversions to
189 quantify the contemporary carbon cycle with the accuracy and precision needed 1) to
190 evaluate and improve terrestrial carbon cycle models, and 2) to monitor carbon fluxes in
191 support of climate-change mitigation efforts. This overarching goal is being pursued via three
192 specific objectives: 1) quantification and reduction of uncertainty in simulations of
193 atmospheric C transport, 2) quantification and reduction in uncertainty in prior C flux
194 estimates, and 3) evaluation of the ability of the OCO-2 instrument to capture regional-scale,
195 tropospheric gradients in column CO_2 (XCO_2). Since the atmospheric and ecosystem
196 processes we are studying are found throughout the Earth's midlatitudes, and the satellite
197 observations we are evaluating are global in scope, our results should improve our ability to
198 diagnose the Earth's carbon cycle on a global scale, and over the decades encompassed by the
199 long-term C observing network. The intersecting elements of the mission are illustrated in
200 Figure 1.

201 ## Instruments and Platforms

202 *Airborne platforms.*

203 Two aircraft, a NASA Langley Research Center Beechcraft B-200 King Air, and a NASA
204 Wallops Flight Facility Lockheed C-130 Hercules, carried a common suite of in situ,

205 continuous sensors measuring meteorological variables (wind speed, wind direction, and
206 atmospheric temperature, water vapor and pressure), aircraft position, atmospheric C mole
207 fractions (Baier et al., 2020), and atmospheric C tracers including carbon monoxide (CO),
208 ozone (O_3), ethane (C_2H_6, Weibring et al., 2020; Kostinek et al., 2019) and approximately 50
209 long-lived trace gases including $^{14}CO_2$ and carbonyl sulfide (OCS) using flask whole-air
210 samplers (Baier et al., 2020). The C-130 carried additional instrumentation, including an in
211 situ nitrous oxide (N_2O) analyzer (Kostinek et al., 2019), a downward-pointing backscatter
212 lidar able to detect clouds and clear-air atmospheric structure including atmospheric
213 boundary layer (ABL) depth (McGill et al., 2004; Pal et al, 2020b), and a downward-pointing
214 integrated path differential absorption (IPDA) lidar to measure either column CO_2 (XCO_2,
215 first four flight campaigns, Campbell et al., 2020) or column CH_4 (XCH_4, aerosol/cloud, and
216 ABL depth, final flight campaign). More details on the instruments, performance metrics,
217 calibration procedures and data archives are found in Wei et al., (2021).

218 *Towers*.

219 Communications towers were instrumented with Picarro cavity ring-down spectrometers
220 to measure C at approximately 100m above ground (Miles et al., 2018). Eleven towers were
221 selected to fill in gaps in the NOAA GGGRN. These towers operated throughout the years
222 (2016-2019) of the ACT-America airborne campaigns.

223 *Satellites*.

224 Fourteen ACT-America flights were coordinated with the passage of OCO-2 such that the
225 aircraft were co-located temporally and spatially within the instrument's measurement swath
226 (Bell et al., 2020). The final ACT-America flight campaign overlapped with operations of
227 the European Space Agency's TROPOMI instrument, which retrieves XCH_4 globally on a
228 daily basis.

Ensemble Modeling System

Ensemble modeling is an essential element of ACT-America's methodology (Figure 1). A transport ensemble consisting of a mesoscale atmospheric transport model with multiple physical parameterizations (Díaz-Isaac et al., 2019), initial conditions (Chen et al., 2019; Feng et al., 2019a,b) and resolutions (Samaddar et al., 2021) is embedded within a suite of global atmospheric C reanalyses (Butler et al., 2020; Feng et al., 2019a,b), and can include an ensemble of ecosystem and anthropogenic C flux estimates (Zhou et al., 2020; Feng et al., 2019a,b). This multi-component ensemble system enables model sensitivity to any of the individual components to be explored independently (e.g. Feng et al., 2019a; 2019b; Chen et al., 2019). This enables ACT-America to address a primary challenge in the study of atmospheric C: the disaggregation of model-data errors caused by surface fluxes vs. atmospheric transport.

The model ensemble provides a realistic assessment of uncertainty only if the range of variation in the components represents our uncertainty in those components. Thus, another critical feature of the ensemble modeling effort is the attempt to calibrate the ensemble vs. both meteorological measurements (Diaz et al., 2019; Feng et al., 2019a,b) and atmospheric C flux and mole fraction observations (Zhou et al., 2020; Feng et al., 2019a,b). We use the term calibration in the sense of carefully determining the range of the ensemble for the purpose of quantifying uncertainty. Minimizing bias is also critical to the quality of the ensemble (Diaz et al., 2019). Continued evaluation and improvement of the model ensembles using ACT-America observations, and applications of the ensembles to improve inversions, is a central focus of ongoing investigation.

In addition to the ensemble, we have created a "baseline simulation" of total atmospheric CO_2 and CH_4 continental enhancements spanning the entire flight campaign (Feng et al.,

253 2020). The C mole fractions are broken down according to their source (e.g. boundaries,
254 fossil, biogenic; Feng et al., 2019b; Barkley et al., 2019a). This baseline simulation has been
255 combined with the HYSPLIT (Stein et al., 2015) and FLEXPART (Pisso et al., 2019)
256 Lagrangian dispersion models to create influence functions for both flask samples (Baier et
257 al., 2020) and continuous aircraft observations (Cui et al., 2021).

258 Flight patterns and campaigns

259 *Flight regions*.

260 We chose ACT-America flight regions to encompass a range of weather and C fluxes.
261 The Midwest region (flight base Lincoln, Nebraska) enabled the sampling of midlatitude
262 cyclones early in their life cycles, and agricultural C fluxes. The South-Central region (flight
263 base Shreveport, Louisiana) featured coastal convection, strong atmospheric influence from
264 the Gulf of Mexico, substantial anthropogenic C fluxes, and forested and agricultural
265 ecosystems with substantially different seasonality than the other study regions. The
266 MidAtlantic region (flight bases NASA Wallops Flight Facility in Chincoteague, Virginia,
267 and NASA Langley Research Center in Hampton, Virginia) spanned the Appalachian
268 temperate forests, large anthropogenic C fluxes, and late-stage weather systems that carried
269 the accumulated signatures of C fluxes from across the continent. These central and eastern
270 U.S. ecosystems are highly productive and encompass a large fraction of US ecosystem and
271 anthropogenic C fluxes and flux uncertainty (Alvarez et al., 2018; Feng et al., 2019b;
272 USGCRP, 2018).

273 *Flight patterns*.

274 ACT-America conducted three types of flights: OCO-2 underflights, fair weather flights
275 and frontal flights. The fair and frontal flights were arranged to construct synoptic sequences

(Figure 2), with flight planning guided by a vigorous daily flight forecasting effort. Both aircraft were deployed for the majority of ACT-America flights. All flights were conducted during late morning through mid-afternoon hours in order to minimize vertical gradients in C within the ABL.

OCO-2 UNDER-FLIGHTS

For OCO-2 under flights, the two aircraft flew out and back along a single track approximately 500 km in length that was within the sampling swath of the satellite (Figure 3). Since OCO-2 measurement retrievals are limited in the presence of cloud fields, clear conditions were targeted. This observation strategy, designed to test the ability of OCO-2 to retrieve regional-scale spatial variability in tropospheric XCO_2, represents a unique contribution (Bell et al., 2020) to the OCO-2 XCO_2 evaluation literature.

SYNOPTIC SEQUENCES

We designed the majority of ACT-America flights to sample the GHG and meteorological properties of midlatitude weather systems. This included multi-level flights across frontal boundaries, and within pre- and post-frontal fair-weather air masses. A sample multi-day flight sequence from the summer of 2016 is illustrated in Figure 4.

Pre-frontal conditions in the US Midwest were sampled on 9 and 10 August (Figure 4a). The fair-weather patterns flown on these two days were designed so that the ABL portion of the 9 August flight was approximately one day's advection upwind of the ABL air sampled on 10 August to enable regional C flux estimates. Flow in the pre-frontal conditions came primarily from the south, but with some northerly air mass history since the flights were close to the high-pressure center (Figure 4f). These two-day sequences were flown primarily in the summer of 2016, and close to the center of fair-weather high-pressure systems whose light

299 winds allowed this quasi-Lagrangian flight plan to be executed. ABL C mole fractions in fair
300 weather were often strikingly heterogeneous (Figure 4a,c), reflecting both spatially
301 heterogeneous fluxes and the variable air mass history found within a high pressure center
302 (Figure 4f).

303 A front moved through the region on 12 August, 2016 and was sampled at four altitudes
304 along a flight track approximately perpendicular to the front (Figure 4e). Large differences in
305 both CO_2 and CH_4 were found across the front in both the ABL and the free troposphere (FT),
306 with larger differences in the ABL (Figure 4d): this was typical of the fronts sampled during
307 this campaign (Pal et al., 2020a). The influence functions (Figure 4g) show the convergence
308 at the front of air masses influenced by C fluxes from the upper MidWest and the South.
309 Persistent cross-frontal C differences were found in all seasons, but were the largest in the
310 summer. This flight also shows an elevated band of CO_2 in the ABL at about -94° to -95°
311 longitude, just ahead of the cold front (Figure 4b, d), a feature common to all frontal crossing
312 flights (Pal et al., 2020a). The large and persistent cross-frontal C mole fraction differences
313 (Pal et al., 2020a) are highly sensitive to regional C fluxes (Hu et al., 2021; Samaddar et al.,
314 2021), and emphasize both the importance of fronts in the meridional transport of C (Schuh et
315 al., 2019) and their value in determining regional C fluxes (Hu et al., 2021; Barkley et al.,
316 2019a).

317 Post-frontal, fair weather flights on 13 and 14 August (Figure 4c) sampled the strong shift
318 to northwesterly winds sensitive to fluxes from the upper MidWest (Figure 4h). ABL C mole
319 fractions remained highly variable (Figure 4c), despite the homogeneous air mass history.

320 The slightly elevated ABL CO_2 in the warm sector and strongly depleted CO_2 in the cold
321 sector (Figure 4a-c) suggest a weak CO_2 source in southern ecosystems and a strong
322 MidWestern ecosystem sink then (Pal et al., 2020a). The free tropospheric cross-frontal mole

fraction differences reflect large-scale seasonal, latitudinal gradients (Pal et al., 2020a). This sequence also illustrates the strong organization of C mole fractions as a function of air mass history associated with the passage of weather systems. Averaging soundings seasonally or regionally without attention to the synoptic state will erase this valuable information about upwind fluxes. Model-data comparisons sampled according to air mass history show more ability to distinguish among simulations of C fluxes and transport than comparisons that average all data (Gerken et al., 2021; Gaudet et al., 2021).

GULF INFLOW FLIGHTS

In all seasons, the Gulf of Mexico provided distinct, homogeneous C upwind boundary conditions for our flights. This continental boundary exhibited itself most strongly in the pre-frontal and warm sector data in the South and MidWest regions. Those air masses had considerably less variability than the air coming from the northwest across a large expanse of the North American continent (Gerken et al., 2021). We took advantage of this simple boundary condition by deploying a number of flights downwind of the Gulf when high pressure systems to the east led to a steady onshore flow (Figure 2). The change in C mole fractions downwind of the Gulf provides another upwind-downwind constraint on regional fluxes in the far southern portion of our study domain.

FAIR WEATHER TRANSECTS.

In order to better capture a large swath of upwind fluxes, and because in the dormant seasons ABL wind speeds were often too high to make a two-day Lagrangian sequence feasible, we changed our flight strategy for fair weather conditions to single flight days with a long, cross-wind transect and a second upwind transect to measure the changes in C mole fractions caused by more local fluxes.

LIDAR OVERPASSES

Nearly every C-130 flight included one to four lidar overpasses of a spiral ascent or descent. Some of these spirals included lidar overpasses at multiple altitudes. These 166 overpasses (a subset after screening for non-ideal conditions) enabled empirical tests and correction for biases in the lidar XCO_2 (Campbell et al., 2020) and XCH_4 observations.

Flight campaign climatology.

Flight campaigns sampled the large seasonality in both weather and ecosystem C fluxes characteristic of the midlatitudes. Flight campaigns (Figure 2) were long enough to capture seasonally-typical flux and weather conditions in each of our three flight regions. Flights were conducted for two weeks in each region, sampling roughly two synoptic sequences per region, and targeted typical rather than extreme conditions. Two summer flight campaigns were conducted both to increase sampling when biogenic CO_2 fluxes are at their peak, and, for the Southern and MidWestern regions, to capture earlier and later summer conditions.

Summer 2016 sampled mid- to late-summer conditions. Climatological conditions were fairly typical in two of our three flight regions. One significant exception was the flooding that occurred in the South, with the most extreme flooding taking place in southern Louisiana (Brown et al., 2020). Our final flight campaign, summer 2019, was conducted in early- to mid-summer conditions and was intended to sample earlier season biogenic CO_2 fluxes a full two months earlier than our summer 2016 campaign in the South, and one month earlier in the MidWest. This plan was complicated by extreme flooding in the late spring of 2019 in the central United States (Yin et al., 2020). The flooding delayed planting of crops in the MidWest by more than two weeks, and the landscape in early July appeared to be roughly a month behind in crop development. The South was not as broadly impacted in terms of

vegetation phenology, though river valleys were flooded all across the region. The MidAtlantic region was sampled at the same time of year in both campaigns. Summer 2019 in the MidAtlantic included a period of extreme heat (17-22 July).

Other seasonal campaigns also included climatological anomalies worthy of mention. The MidWestern portion of the winter 2017 flight campaign encountered anomalously warm conditions from 13-18 February, approximately the first week of flights. The regional surface remained snow-covered and the warm air and snow-covered surface resulted in very shallow boundary layers until a strong storm system on 20 February, the center-point of one of the synoptic sequences sampled by ACT (Figure 2), brought a return to more typical regional weather conditions. The MidAtlantic winter campaign (27 February - 10 March) coincided with an early spring. Snowmelt had already occurred over most of the region. Exposed soils and lack of any significant transpiration from vegetation led to high sensible heat fluxes and some very deep ABLs (1-10 March), as is typical of the period between snowmelt and green-up in this region.

The fall 2017 campaign was climatologically typical across all regions. The Southern region retained some leaf cover and photosynthetic activity, while the other regions were mostly senescent. Atmospheric boundary layers were well-defined, and we encountered a number of relatively clear, dry frontal passages. One notable weather event was the passage through our study region of Hurricane Nate on 8-10 October. We did not deploy research flights to study the hurricane, choosing to sample the more common midlatitude cyclones, but MidAtlantic region flights did take place before and after the hurricane passage.

The spring 2018 campaign followed an unusually snowy winter and late greening in the MidWest. Flights over the MidWest included some snow-covered terrain, and no appreciable photosynthetic activity. Flights in Southern and MidAtlantic regions spanned the boundary

393 of the vegetation greening. The greening was quite evident in the atmospheric data, with
394 readily observed changes in ABL CO_2 that were correlated with the boundary of vegetation
395 greenness (Figure 5). The other notable weather condition for the campaign was the presence
396 of two stationary fronts, one that extended from the Gulf to the upper MidWest and persisted
397 over this region from 30 April through 3 May. We sampled the stationary front 3 times from
398 our MidWestern flight base (Figure 2). The other stationary front was west to east in
399 orientation, and persisted over the MidAtlantic region from 11-18 May. Five flights sampled
400 this front. These multi-day case studies are ripe for case studies, including strong biological
401 flux contrasts and active atmospheric mixing.

402 **Analyses**

403 *Carbon weather observational metrics.*

404 Denning et al., (1995), Stephens et al., (2007), Pickett-Heaps et al., (2011) and Thompson
405 et al., (2016) have all illustrated the value of evaluating atmospheric inversion systems using
406 vertical C profiles. Inspired by this past work, and following the working hypothesis that
407 accurate understanding of C mole fractions within mid-latitude weather systems is essential
408 for accurate atmospheric inversions, we have developed new metrics focusing on the
409 synoptic-scale performance of atmospheric C simulation and inversion systems.

410 Pal et al., (2020a) demonstrated a set of metrics that quantify cross-frontal C mole
411 fraction differences as a function of tropospheric layer (ABL, lower FT, upper FT), and
412 vertical differences in C mole fractions between these layers within the cold (postfrontal) and
413 warm (prefrontal) air masses. Pal et al., (2020a) show that these metrics are highly consistent
414 within a season across the entire central and eastern U.S. Gerken et al., (2021) expanded this
415 approach to include probability distributions and spatial variograms of model-data differences

in CO_2 mole fractions within these atmospheric sectors. Gerken et al., (2021) illustrate that, when averaged across season, region altitude and air mass, model-data comparisons of CO_2 may show relatively little bias, but that when data are disaggregated by altitude and air mass, systematic biases appear.

We have included diagnostic flags in the ACT-America in situ observations to enable analyses that are oriented with respect to these synoptic metrics (Davis et al., 2018). All in situ aircraft data were complemented with three flags which identify whether or not the observations are within the ABL, the air mass position of the data point (warm / prefrontal, cold / postfrontal or ambiguous), and the aircraft maneuver (level leg, takeoff, landing, spiral ascent/descent, en route ascent/descent). Flags exist for every ACT-America in situ data point and these are integrated into the flight data stored at the Oak Ridge DAAC (Wei et al., 2021; Davis et al., 2018) and as an additional download accompanying NOAA's ObsPack product (Schuldt et al., 2020).

OCO-2 tropospheric XCO_2 variability

Multiple OCO-2 under flights were evaluated by Bell et al. (2020). Spatial gradients in tropospheric XCO_2 across the few- to several-hundred-kilometer flight paths differed by 0.1 ppm per 100 km or less among three XCO_2 estimates. These results suggest that regional structures in OCO-2 XCO_2 can be used to inform regional-scale flux inversions, and are motivating both direct observational analysis of synoptic scale variations in XCO_2 (Wang et al., 2021), and new descriptions of OCO-2 XCO_2 uncertainty structure in atmospheric inversions (Baker et al., 2021). Higher resolution inversion systems may be needed to take full advantage of this information.

Seasonal, regional flux evaluation

ACT-America flight data are being used to evaluate C fluxes in two ways. First, multiple C flux estimates, including ACT-America's CASA-based CO_2 flux ensemble (Zhou et al., 2020), have been propagated forward in our baseline WRF simulation. These simulated atmospheric C mole fractions can be compared to ACT-America airborne data to identify the most plausible ensemble members (e.g. Feng et al., 2021). Case studies exploring realizations of the Vegetation Photosynthesis and Respiration Model (VPRM) have also been performed (Hu et al., 2021). Flux estimates can also be adjusted to maximize the fit to the ACT-America observations (e.g. Barkley et al., 2019a, b). Second, back-trajectory Lagrangian influence functions (Cui et al., 2021) created with the WRF baseline simulation can be convolved with flux estimates to estimate atmospheric C at the locations of aircraft observations. These model-data differences can be used to evaluate regional, seasonal flux estimates, including terrestrial biosphere models (Parazoo et al., 2021) and posterior fluxes from atmospheric inversions (Cui et al., 2021). The influence functions enable any flux estimates to be evaluated without requiring them to be coupled to a new atmospheric transport simulation.

Boundary conditions

These C flux evaluations require treatment of C transport from outside the region of interest. Atmospheric C mole fractions within our study domain can be expressed, following Feng et al. (2019b), as

$$C_{tot} = C_b + \sum_i C_i, \qquad (1)$$

where C_{tot} is the total atmospheric mole fraction, C_b is the mole fraction transported from outside of the study region, and C_i are the mole fraction contributions from sources or sinks, i, within the study region. ACT-America has developed two independent approaches to determining C_b so that aircraft or tower observations can be used to study continental fluxes.

First, we have merged boundary conditions from global C inversion systems into our continental-scale WRF simulation domain (Butler et al., 2020). We have included multiple versions of global boundary conditions to account for uncertainty in these background conditions (Feng et al., 2019b). Background conditions account for most of the C in the atmosphere of North America, but comparison of global inversion systems shows that the uncertainty in these boundary conditions is modest, typically of order 1 ppm for CO_2, compared to continental fluxes that account for several to tens of ppm of CO_2 for continental fluxes (Feng et al., 2019a,b; Chen et al., 2019). A second approach is to assume that inflow from outside of the continent is homogeneous in the vertical, and that deep vertical mixing over the continent is limited so that upper free tropospheric mole fraction measurements are approximately equal to continental background conditions (Parazoo et al., 2021). NOAA aircraft profiling on the Pacific and Gulf coasts (Sweeney et al., 2015), ACT-America profiles over the Gulf (e.g. Campbell et al., 2020) and model-data comparisons in the upper free troposphere (Gerken et al., 2021) suggest that this is a reasonable approximation. Comparison of these approaches and more extensive quantification of this source of uncertainty is worthwhile.

A third background scenario emerges in the attempt to isolate regional to local, not continental-scale, fluxes. In this case, free tropospheric mole fractions are not a suitable background condition (Turnbull et al., 2015). Instead ABL mole fractions outside of the influence of the region of interest are matched with simulations of both background mole fractions and fluxes from outside the region of interest to isolate mole fraction enhancements from the region of interest (Barkley et al., 2017). This approach is difficult to apply to biogenic CO_2 fluxes, since they are so broadly distributed, but this method works well for

485 studying emissions from discrete source regions such as cities or anthropogenic CH_4
486 emissions (Barkley et al., 2019a; 2021) and agricultural N_2O emissions (Eckl et al., 2021).

487 Quantifying regional, seasonal fluxes also benefits from the ability to segregate
488 component fluxes. We can do this with both numerical and observational approaches. Our
489 WRF simulations include C mole fractions for each source or sink sector, making it possible
490 to segregate, for example, atmospheric CO_2 mole fractions originating from continental fossil
491 fuel vs. biogenic CO_2 fluxes (Feng et al., 2019a,b; Hu et al, 2021; Samaddar et al., 2021), and
492 atmospheric CH_4 mole fractions originating from continental or regional oil and gas vs. coal
493 vs. agricultural emissions (Barkley et al., 2019a, b). If the uncertainty in one particular source
494 is known with more confidence, simulated sector mole fractions, C_i, can be subtracted from
495 the observed total mole fraction, C_{tot}, to isolate the sector mole fraction of interest. Calibrated
496 ensembles (Feng et al., 2019b) can be used to address uncertainty in the sectoral fluxes.

497 As a complement to these numerical methods, we measured CO and $^{14}CO_2$ to isolate
498 fossil fuel CO_2 mole fractions (Baier et al., 2020), OCS to segregate photosynthetic vs.
499 respiratory biogenic CO_2 fluxes (Parazoo et al., 2021), and ethane (C_2H_6) to segregate
500 thermogenic from biogenic CH_4 sources (Barkley et al., 2019a, b; 2021). Figure 7 shows an
501 example of such an analysis applied to estimating regional CH_4 emissions from the southern
502 United States.

503 ACT's lidar-based column C measurements have a unique capability to constrain regional
504 C fluxes that has yet to be demonstrated. These observations, combined with backscatter lidar
505 ABL depth measurements, can be used to infer regional GHG fluxes without concerns about
506 the ability of in situ aircraft data to properly capture the vertical distribution of GHGs within
507 the ABL.

Evaluation of atmospheric inversions

Disaggregating the influence of flux and transport on a given atmospheric C mole fraction measurement has been a challenge for atmospheric inversions for decades. ACT-America's observation of the structures of C mole fractions within weather systems provides a strong basis for untangling the interdependency of midlatitude weather and fluxes.

Multiple avenues of inversion system evaluation are being explored. Evaluation of atmospheric transport variables, atmospheric C mole fractions (Gaudet et al., 2021), and posterior fluxes (Cui et al., 2021) from the global-scale OCO-2 Model Intercomparison Project (OCO2 MIP, Crowell et al., 2019) is underway in an attempt to identify the inversion systems that are most consistent with ACT-America's carbon weather metrics. The same metrics will be used to evaluate continental atmospheric inversions, such as CarbonTracker-Lagrange (Hu et al., 2019), once these become available. Model studies that control for sources of variability among inversions are also underway in an attempt to identify the causes of model-data discrepancies. Studies of this sort include studies of the impact of model resolution (Samaddar et al., 2021) and atmospheric transport model (Gerken et al., 2021), both using common fluxes to isolate the impact of transport on CO_2 mole fractions. More controlled model experiments confronted with ACT-America observations are needed to close our understanding of midlatitude C weather and the impact of the simulation of C weather on C flux inversions.

The ensemble modeling initiated by ACT-America (Chen et al., 2019; Feng et al., 2019a,b; 2021) illustrates another path to improving atmospheric inversions. Figure 7 shows the variability in ABL CO_2 mole fractions produced by elements of a calibrated C model ensemble (Feng et al., 2019b). Ensembles like these, if calibrated and verified with intensive regional observations like ACT-America flights, can identify those regions and times where

flux uncertainty is large and other sources of uncertainty are small, and direct atmospheric inversion systems to use those data preferentially to solve for regional C fluxes.

Improvement of atmospheric C inversions.

In addition to evaluating existing atmospheric inversion systems using the aircraft data as independent observations, we have begun to translate our results into improvements in regional and global atmospheric inversions. Avenues for improvement of the inversion systems include modifying the assumptions about local to regional-scale errors and error correlations in OCO-2 observations (Baker et al., 2021), minimizing biases and adjusting uncertainties in prior fluxes used in inversions based on evaluation of these flux models (e.g. Barkley et al., 2019a, 2021; Feng et al., 2021), and improving atmospheric transport field and transport uncertainty assessments (Gerken et al., 2021; Feng et al., 2019a; Lauvaux et al., 2019). These advances have yet to be tested in established inversion systems. ACT-America has also begun to develop new inversion systems that can incorporate prior flux (Wesloh et al., 2020) and atmospheric transport (Lauvaux et al., 2019) ensemble information.

Conclusions

ACT-America's observational record provides unparalleled insight into the C fluxes and mole fractions of midlatitude weather systems - the carbon weather of the midlatitudes. We have confirmed that midlatitude weather systems are clearly responsible for a large component of the spatial and temporal variability in atmospheric C mole fractions over the continents, and have shown the strong connection between this weather-scale variability and terrestrial C fluxes. Modeling and analysis systems that can properly resolve these weather systems and interpret these carbon weather signals will provide superior regional and

554 continental C flux estimates. Analyses that neglect the role of weather systems in C transport
555 run the risk of masking compensating errors that will bias their results.

556 More work is needed to untangle the mixed influences of C flux and transport
557 uncertainties at sub-continental scales in current atmospheric inversion systems. ACT-
558 America investigations have pioneered new approaches in ensemble C simulations which,
559 combined with ACT-America's airborne database, are beginning to isolate and quantify the
560 impact of flux versus transport errors. These methods, as they are adopted in atmospheric
561 inversions, should continue to improve the accuracy and precision of regional inverse flux
562 estimates.

563 We have demonstrated that column remote sensing technologies, both space- and air-
564 borne, have the precision and stability needed to document regional-scale atmospheric C
565 gradients. These findings show promise for continued use of both passive and active remote
566 sensing in the study of C mole fractions and fluxes.

567 An unparalleled airborne methane and ethane dataset enabled us to make strong progress
568 in evaluating anthropogenic emissions of CH_4 from the central and eastern US. We have
569 begun to use the airborne data set to evaluate and improve seasonal and regional terrestrial
570 biosphere model CO_2 flux estimates. Much more can be done in this area.

571 Independent, routine, atmospheric evaluation of models and inventories of C fluxes at
572 spatial domains of geopolitical and ecological relevance remains an important need for
573 climate science and climate change mitigation. This is rapidly becoming feasible for fossil
574 fuel CO_2 emissions and some anthropogenic CH_4 emissions. This is more challenging for
575 broadly distributed fluxes such as agricultural and wetland CH_4 emissions, and biogenic CO_2
576 fluxes. ACT-America investigations have provided an observation and methodological
577 framework that will enable this advance.

578

579 *Acknowledgments*.

580 The ACT-America project is a NASA Earth Venture Suborbital 2 project funded by
581 NASA's Earth Science Division. Authors were supported by the following NASA grants:
582 NNX15AG76G to Penn State (Davis); NNX15AJ06G (Baier, Sweeney) and NNX15AW47G
583 (Fried) to University of Colorado-Boulder; NNX16AN17G to Clark University (Williams);
584 NNL15AQ00B to Exelis (Dobler); 80NSSC19K0730 to Texas Tech and a Texas Tech
585 University start up research grant (Pal); NNX15AI97G (O'Dell), NNX15AJ07G (D. Baker,
586 Schuh), NNX15AJ09G (Denning), and 80NSSC20K0924 (I. Baker) to Colorado State
587 University; NNX17AG11G (Xue) to U. Oklahoma. Additional support for research was
588 provided by NASA grants NNX12AP90G (Davis), NNX14AJ17G (Davis), NNX14AL32H
589 (Normile) and NNX13AP34G (Lauvaux). Complementary support for tower-based
590 measurements was provided by NASA grant NNX14AJ17G and NIST grant
591 70NANB15H336. The ORNL DAAC is sponsored by the National Aeronautics and Space
592 Administration under Interagency Agreement 80GSFC19T0039. ORNL participation in
593 ACT-America was funded by interagency agreement NNL15AA10I. NASA co-authors were
594 supported by NASA Science Mission Directorate funding awarded in response to the Earth
595 Venture Suborbital-2 Announcement of Opportunity NNH13ZDA001N-EVS2. Roiger was
596 supported by DLR VO-R via the young investigator research group "Greenhouse Gases." T.
597 Lauvaux was supported by the French research program Make Our Planet Great Again
598 (project CIUDAD).

599 The authors acknowledge NASA's Earth System Science Pathfinder Program Office,
600 NASA's Airborne Sciences Program, NASA's Atmospheric Science Data Center, and
601 NASA's Pleiades supercomputing facilities, as well as the administrative and flight

602 forecasting support from Penn State's Department of Meteorology and Atmospheric
603 Sciences. The project would not have been possible without the dedicated and tireless support
604 of the many employees of these institutions and facilities.

605

606 *Data Availability Statement*.

607 ACT-America observational and modeling data sets are archived at the ORNL DAAC
608 (https://actamerica.ornl.gov/) and are open to use by any investigator without restriction. CO_2
609 and CH_4 observations are also available through NOAA's ObsPack (Masarie et al, 2014) data
610 set (https://www.esrl.noaa.gov/gmd/ccgg/obspack/). Numerical modeling products not yet
611 available at the ORNL DAAC are available through Penn State Data Commons.

612

613 REFERENCES

614 Agustí-Panareda, A., and Coauthors, 2019: Modelling CO_2 weather – why horizontal
615 resolution matters. *Atmos. Chem. Phys.*, **19**(11), 7347–7376. https://doi.org/10.5194/acp-
616 19-7347-2019.

617 Alvarez, R. A., and Coauthors, 2018: Assessment of methane emissions from the U.S. oil and
618 gas supply chain. *Science,* **361**, 186-188, doi:10.1126/science.aar7204.

619 Andrews, A. E., and Coauthors, 2014: CO_2, CO, and CH_4 measurements from tall towers in
620 the NOAA Earth System Research Laboratory's Global Greenhouse Gas Reference
621 Network: instrumentation, uncertainty analysis, and recommendations for future high-
622 accuracy greenhouse gas monitoring efforts. *Atmos. Meas. Tech.*, **7**(2), 647–687.
623 https://doi.org/10.5194/amt-7-647-2014.

624 Baier, B. C., and Coauthors, 2020: Multi-species assessment of factors influencing regional
625 CO_2 and CH_4 enhancements during the wintertime ACT-America campaign. *J. Geophys.*
626 *Res.: Atmos.*, **125**, e2019JD031339. https://doi.org/10.1029/2019JD031339.

627 Baker, D.F., Bell, E., Davis, K.J., Campbell, J.F., Lin, B., and Dobler, J., 2021: Calculating
628 an error correlation length scale from MFLL-OCO2 column-average CO_2 differences and
629 using it to average OCO-2 data. In review, *Geosci. Model Dev.,*
630 https://www.essoar.org/doi/pdf/10.1002/essoar.10505688.1.

631 Baker, D.F., H. Bösch, S.C. Doney, D. O'Brien, and D.S. Schimel, 2010: Carbon source/sink
632 information provided by column CO_2 measurements from the Orbiting Carbon
633 Observatory. *Atmos. Chem. Phys.*, **10**, 4145-4165. doi:10.5194/acp-10-4145-2010.

634 Baker, D.F., S.C. Doney, and D.S. Schimel, 2006a: Variational data assimilation for
635 atmospheric CO_2, *Tellus-B,* **58** (5), 359-365, doi:10.1111/j.1600-0889.2006.00218.x.

636 Baker, D. F., and Coauthors, 2006b: TransCom 3 inversion intercomparison: Impact of
637 transport model errors on the interannual variability of regional CO_2 fluxes, 1988-2003,
638 *Global Biogeochem. Cycles*, **20**, GB1002, doi:10.1029/2004GB002439.

639 Barkley, Z. R., and Coauthors, 2021: Analysis of Oil and Gas Ethane and Methane Emissions
640 in the Southcentral and Eastern United States Using Four Seasons of Continuous Aircraft
641 Ethane Measurements. In review, *J. Geophys. Res.: Atmos.*,
642 https://www.essoar.org/doi/10.1002/essoar.10505536.1.

643 Barkley, Z. R., K. J. Davis, S. Feng, N. Balashov, A. Fried, J. DiGangi, Y. Choi, and H. S.
644 Halliday, 2019a: Forward Modeling and Optimization of Methane Emissions in the South
645 Central United States Using Aircraft Transects Across Frontal Boundaries. *Geophys. Res.*
646 *Lett.*, **46**, 13,564–13,573. https://doi.org/10.1029/2019GL084495.

647 Barkley, Z. R., and Coauthors, 2019b: Estimating methane emissions from underground coal
648 and natural gas production in southwestern Pennsylvania, *Geophys. Res. Lett.*, **46**, 4531-
649 4540, https://doi.org/10.1029/2019GL082131.

650 Barkley, Z. R., and Coauthors, 2017: Quantifying methane emissions from natural gas
651 production in north-eastern Pennsylvania, *Atmos. Chem. Phys.*, **17**, 13941–13966,
652 https://doi.org/10.5194/acp-17-13941-2017.

653 Barnes, E. A., N. Parazoo, C. Orbe and A. S. Denning, 2016: Isentropic transport and the
654 seasonal cycle amplitude of CO_2, *J. Geophys. Res.: Atmos.*, **121**, 8106–8124,
655 doi:10.1002/2016JD025109.

656 Battle, M., M. L. Bender, P. P. Tans, J. W. C. White, J. T. Ellis, T. Conway, R. J. Francey,
657 2000: Global carbon sinks and their variability inferred from atmospheric O_2 and $\delta^{13}C$.
658 *Science*, **287**, 2467-2470.

659 Bell, E., and Coauthors, 2020: Evaluation of OCO-2 XCO_2 variability at local and synoptic
660 scales using lidar and in situ observations from the ACT-America campaigns. *J.*
661 *Geophys. Res.: Atmos.*, **125**, e2019JD031400. https://doi.org/10.1029/2019JD031400.

662 Bloom, A.A., K. Bowman, M. Lee, A.J. Turner, R. Schroeder, J.R. Worden, R.J. Weidner,
663 K.C. McDonald, and D.J. Jacob, 2017: CMS: Global 0.5-deg Wetland Methane
664 Emissions and Uncertainty (WetCHARTs v1.0). ORNL DAAC, Oak Ridge, Tennessee,
665 USA. https://doi.org/10.3334/ORNLDAAC/1502.

666 Bousquet, P., and Coauthors, 2006: Contribution of anthropogenic and natural sources to
667 atmospheric methane variability. *Nature*, **443**, 439-443.

668 Brown, V., B. D. Keim, W. D. Kappel, D. M. Hultstrand , A. G. Peyrefitte Jr., A. W. Black,
669 K. M. Steinhilber, and G. A. Muhlestein, 2020: How rare was the August 2016 south-

central Louisiana heavy rainfall event? *J. Hydrometeor.*, **21**, 773-790, https://doi.org/10.1175/JHM-D-19-0225.1.

Bruhwiler, L. M., et al. (2017), U.S. CH4 emissions from oil and gas production: Have recent large increases been detected?, J. Geophys. Res. Atmos., 122, 4070–4083, doi:10.1002/2016JD026157.

Butler, M. P., T. Lauvaux, S. Feng, J. Liu, K. W. Bowman, and K. J. Davis, 2020: Atmospheric simulations of total column CO_2 mole fractions from global to mesoscale within the Carbon Monitoring System Flux inversion framework. *Atmosphere*, **11**, 787; doi:10.3390/atmos11080787.

Campbell, J. F., and Coauthors, 2020: Field evaluation of column CO_2 retrievals from intensity- modulated continuous-wave differential absorption lidar measurements during the ACT-America campaign. *Earth Space Sci.*, **7**, e2019EA000847, https://doi.org/10.1029/2019EA000847.

Chan, D., M. Ishizawa, K. Higuchi, S. Maksyutov, and J. Chen, 2008: Seasonal CO_2 rectifier effect and large-scale extratropical atmospheric transport. *J. Geophys. Res.: Atmos.*, **113**, https://doi.org/10.1029/2007JD009443.

Chen, H. W., F. Zhang, T. Lauvaux, K. J. Davis, S. Feng, M. P. Butler, and R. B. Alley, 2019: Characterization of Regional-Scale CO_2 Transport Uncertainties in an Ensemble with Flow-Dependent Transport Errors. *Geophys. Res. Lett.*, **46**, 4049–4058, https://doi.org/10.1029/2018GL081341.

Chevallier, F., L. Feng, H. Bösch, P. I. Palmer, and P. J. Rayner, 2010: On the impact of transport model errors for the estimation of CO_2 surface fluxes from GOSAT observations, *Geophys. Res. Lett.*, **37**, L21803, https://doi.org/10.1029/2010GL044652.

693 Ciais, P., and Coauthors, 2013: Carbon and Other Biogeochemical Cycles. In: *Climate*
694 *Change 2013: The Physical Science Basis. Contribution of Working Group I to the Fifth*
695 *Assessment Report of the Intergovernmental Panel on Climate Change* [Stocker, T.F., D.
696 Qin, G.-K. Plattner, M. Tignor, S.K. Allen, J. Boschung, A. Nauels, Y. Xia, V. Bex and
697 P.M. Midgley (eds.)]. Cambridge University Press, Cambridge, United Kingdom and
698 New York, NY, USA.

699 Ciais, P., P. Tans, M. Trolier, J.W.C. White, and R.J. Francey, 1995: A Large Northern
700 Hemisphere Terrestrial CO_2 Sink Indicated by the 13C/12C Ratio of Atmospheric CO_2.
701 *Science*, **269**, 1098-1102. doi:10.1126/science.269.5227.1098.

702 Conway, T. J., P. P. Tans, L. S. Waterman and K. W. Thoning, 1994: Evidence for
703 interannual variability of the carbon-cycle from the National Oceanic and Atmospheric
704 Administration Climate Monitoring and Diagnostics Laboratory Global Air Sampling
705 Network. *J. Geophys. Res.: Atmos.*, **99**, 22,831-22,855.

706 Crisp, D., and Coauthors, 2017: The on-orbit performance of the Orbiting Carbon
707 Observatory-2 (OCO-2) instrument and its radiometrically calibrated products, *Atmos.*
708 *Meas. Tech.*, **10**, 59–81, https://doi.org/10.5194/amt-10-59-2017.

709 Crowell, S., and Coauthors, 2019: The 2015-2016 carbon cycle as seen from OCO-2 and the
710 global in situ network, *Atm. Chem. Phys.*, **19**, 9797-9831, https://doi.org/10.5194/acp-19-
711 9797-2019.

712 Cui, Y. Y., A. R. Jacobson, S. Feng, D. Wesloh, T. Gerken, Z. R. Barkley, K. Keller, D.
713 Baker, and K. J. Davis, 2021: Evaluation of inverse estimates of North American net
714 ecosystem exchange of CO_2 from different observing systems using ACT-America

715 airborne observations. In review, *J. Geophys. Res.: Atmos.*,
716 https://www.essoar.org/doi/pdf/10.1002/essoar.10505569.1.

717 Davis, K.J., and Coauthors, 2018: ACT-America: L3 Merged In Situ Atmospheric Trace
718 Gases and Flask Data, Eastern USA. ORNL DAAC, Oak Ridge, Tennessee, USA.
719 https://doi.org/10.3334/ORNLDAAC/1593.

720 Denning, A. S., I. Y. Fung, and D. Randall, 1995: Latitudinal gradient of atmospheric CO_2
721 due to seasonal exchange with land biota, *Nature*, **376**, 240-243.

722 Díaz-Isaac, L. I., T. Lauvaux, M. Bocquet, and K. J. Davis, 2019: Calibration of a multi-
723 physics ensemble for estimating the uncertainty of a greenhouse gas atmospheric
724 transport model, *Atmos. Chem. Phys.*, **19**, 5695-5718, https://doi.org/10.5194/acp-19-
725 5695-2019.

726 Díaz-Isaac, Liza I., T. Lauvaux, and K.J. Davis, 2018: Impact of physical parameterizations
727 and initial conditions on simulated atmospheric transport and CO_2 mole fractions in the
728 US Midwest. *Atmos. Chem. Phys.*, **18**, 14813–14835, doi.org/10.5194/acp-18-14813-
729 2018.

730 Dlugokencky, E. J., and Coauthors, 2011: Global atmospheric methane: budget, changes and
731 dangers. *Philos. Trans. R. Soc. A*, **369**(1943): 2058-2072.

732 Dlugokencky, E. J., R. C. Myers, P. M. Lang, K. A. Masarie, A. M. Crotwell, K. W. Thoning,
733 B. D. Hall, J. W. Elkins, and L. P. Steele, 2005: Conversion of NOAA atmospheric dry
734 air CH_4 mole fractions to a gravimetrically prepared standard scale, *J. Geophys. Res.:*
735 *Atmos.*, **110**, D18306, 10.1029/2005JD006035.

Eckl, M., and Coauthors, 2021: Quantifying nitrous oxide emissions in the U.S. Midwest - A top-down study using high resolution airborne in situ observations, In review, *Geophys. Res. Lett.*, https://www.essoar.org/doi/10.1002/essoar.10505675.1.

Eldering, A., T. E. Taylor, C. W. O'Dell, and R. Pavlick, 2019: The OCO-3 mission: measurement objectives and expected performance based on 1 year of simulated data, *Atmos. Meas. Tech.*, **12**, 2341-2370, https://doi.org/10.5194/amt-12-2341-2019.

Feng, S., T. Lauvaux, C. A. Williams, K. J. Davis, Y. Zhou, I. Baker, Z. R. Barkley and D. Wesloh, 2021: Joint CO_2 Mole Fraction and Flux Analysis Confirms Missing Processes in CASA Terrestrial Carbon Uptake over North America. In review, *Global Biogeochem. Cycles*, https://www.essoar.org/doi/abs/10.1002/essoar.10505330.1.

Feng, S., T. Lauvaux, Z. R. Barkley, K. J. Davis, M. B. Butler, A. Deng, B. Gaudet, D. Stauffer, 2020: Full WRF-Chem output in support of the NASA Atmospheric Carbon and Transport (ACT)-America project (7/1/2016 – 7/31/2019). The Pennsylvania State University Data Commons, University Park, Pennsylvania, USA, https://doi.org/10.26208/49kd-b637.

Feng, S., T. Lauvaux, K. Keller, K. J. Davis, P. Rayner, T. Oda, and K. R. Gurney, 2019a: A Road Map for Improving the Treatment of Uncertainties in High-Resolution Regional Carbon Flux Inverse Estimates. *Geophys. Res. Lett.*, **46**(22), 13461–13469. https://doi.org/10.1029/2019GL082987.

Feng, S., T. Lauvaux, K. J. Davis, K. Keller, Y. Zhou, C. Williams, A. Schuh, J. Liu, I. Baker, 2019b: Seasonal Characteristics of Model Uncertainties From Biogenic Fluxes, Transport, and Large-Scale Boundary Inflow in Atmospheric CO_2 Simulations Over

North America. *J. Geophys. Res.: Atmos.*, **124**(24), 14325–14346. https://doi.org/10.1029/2019JD031165.

Fisher, J.B., D.N. Huntzinger, C.R. Schwalm, and S. Sitch, 2014: Modeling the terrestrial biosphere, *Ann. Rev. Env. Res.*, **39**, 91-123, doi:10.1146/annurev-environ-012913-093456.

Friedlingstein, P., M. Meinshausen, V. K. Arora, C. D. Jones, A. Anav, S. K. Liddicoat, and R. Knutti, 2014: Uncertainties in CMIP5 Climate Projections due to Carbon Cycle Feedbacks. *J. Climate*, **27**(2), 511–526. https://doi.org/10.1175/JCLI-D-12-00579.1.

Gaudet, B. J., K. J. Davis, S. Pal, A.R. Jacobson, A. Schuh, T. Lauvaux, S. Feng and E.V. Browell, 2021: Regional-scale, sector-specific evaluation of global CO_2 inversion models using aircraft data from the ACT-America project. In review, *J. Geophys. Res.: Atmos.*, https://www.essoar.org/doi/pdf/10.1002/essoar.10505705.1.

Gerbig, C., S. Körner, and J. C. Lin, 2008: Vertical mixing in atmospheric tracer transport models: error characterization and propagation, *Atmos. Chem. Phys.*, **8**(3), 591–602, doi:10.5194/acp-8-591-2008.

Gerken, T., S. Feng, K. Keller, T. Lauvaux, J. P. DiGangi, Y. Choi, B. Baier and K. J. Davis, 2021: Examining CO_2 model observation residuals and their implications for carbon fluxes and transport using ACT-America observations. In review, *J. Geophys. Res.: Atmos.*, https://www.essoar.org/doi/abs/10.1002/essoar.10505673.1.

Gregory, J. M., C. D. Jones, P. Cadule, P. Friedlingstein, 2009: Quantifying carbon cycle feedbacks, *J. Climate*, **22**, 5232-5250. DOI: 10.1175/2009JCLI2949.1.

Hazan, L., J. Tarniewicz, M. Ramonet, O. Laurent, and A. Abbaris, 2016: Automatic processing of atmospheric CO_2 and CH_4 mole fractions at the ICOS Atmosphere

781 Thematic Centre, *Atmos. Meas. Tech.*, **9**, 4719–4736, https://doi.org/10.5194/amt-9-4719-
782 2016.

783 Holden, P. B., and Coauthors, 2018: Climate–carbon cycle uncertainties and the Paris
784 Agreement. *Nature Climate Change*, **8**(7), 609–613. https://doi.org/10.1038/s41558-018-
785 0197-7.

786 Hu, H., and Coauthors, 2018: Toward global mapping of methane with TROPOMI: First
787 results and intersatellite comparison to GOSAT. *Geophys. Res. Lett.*, **45**, 3682– 3689.
788 https://doi.org/10.1002/2018GL077259.

789 Hu, L., and Coauthors, 2019: Enhanced North American carbon uptake associated with El
790 Niño. *Science Advances*, **5**(6), eaaw0076. https://doi.org/10.1126/sciadv.aaw0076.

791 Hu, X.-M., S. M. Gourdji, K. J. Davis, Q. Wang, Y. Zhang, M. Xue, S. Feng, B. Moore, and
792 S. M. R. Crowell, 2021: Implementation of improved parameterization of terrestrial flux
793 in WRF-VPRM improves the simulation of nighttime CO_2 peaks and a daytime CO_2 band
794 ahead of a cold front, In review, *J. Geophy. Res.: Atmos.*,
795 https://www.essoar.org/doi/pdf/10.1002/essoar.10505689.1.

796 Huntzinger, D. N., and Coauthors, 2017: Uncertainty in the response of terrestrial carbon sink
797 to environmental drivers undermines carbon-climate feedback predictions, *Scientific*
798 *Reports*, **7**:4765, doi:10.1038/s41598-017-03818-2.

799 Huntzinger, D. N., 2012: North American Carbon Program (NACP) regional interim
800 synthesis: Terrestrial biosphere model intercomparison. *Ecol. Modell.*, **232**, 144-157,
801 doi:10.1016/j.ecolmodel.2012.02.004.

802 Hurwitz, M.D., D.M. Ricciuto, K.J. Davis, W. Wang, C. Yi, M.P. Butler, P.S. Bakwin, 2004:
803 Advection of carbon dioxide in the presence of storm systems over a northern Wisconsin
804 forest. *J. Atmos. Sci.*, **61**, 607-618.

805 Kostinek, J., and Coauthors, 2019: Modification, Characterization and Evaluation of a
806 Quantum/Interband Cascade Laser Spectrometer for simultaneous airborne in situ
807 observation of CH_4, C_2H_6, CO_2, CO and N_2O, *Atmos. Meas. Tech.*, **12**, 1767-1783,
808 https://doi.org/10.5194/amt-12-1767-2019.

809 Kuze et al., 2016: Update on GOSAT TANSO-FTS performance, operations, and data
810 products after more than 6 years in space, 2016: *Atmos. Meas. Tech.*, **9**, 2445–2461,
811 https://doi.org/10.5194/amt-9-2445-2016.

812 Lan, X. and Coauthors, 2019: Long-Term Measurements Show Little Evidence for Large
813 Increases in Total U.S. Methane Emissions Over the Past Decade, *Geophys. Res. Lett.*,
814 **46**, 9, 4991-4999, 10.1029/2018GL081731.

815 Lauvaux, T., L. I. Díaz-Isaac, M. Bocquet, and N. Bousserez, 2019: Diagnosing spatial error
816 structures in CO_2 mole fractions and XCO_2 column mole fractions from atmospheric
817 transport, *Atmos. Chem. Phys.*, **19**, 12007–12024, https://doi.org/10.5194/acp-19-12007-
818 2019.

819 Lauvaux, T., and K. J. Davis, 2014: Planetary boundary layer errors in mesoscale inversions
820 of column-integrated CO_2 measurements, *J. Geophys. Res.: Atmos.*, **119**, 490–508,
821 doi:10.1002/2013JD020175.

822 Lauvaux, T., and Coauthors, 2012: Constraining the CO_2 budget of the corn belt: exploring
823 uncertainties from the assumptions in a mesoscale inverse system, *Atmos. Chem. Phys.*,
824 **12**, 337-354.

825 Liu, J., and Coauthors, 2017: Contrasting carbon cycle responses of the tropical continents to
826 the 2015-2016 El Nino. *Science*. **358**(6360), eaam5690. DOI: 10.1126/science.aam5690.

827 Machida; T., and Coauthors, 2008: Worldwide Measurements of Atmospheric CO_2 and Other
828 Trace Gas Species Using Commercial Airlines. *J. Atmos. Oceanic Technol.,* **25** (10):
829 1744–1754. https://doi.org/10.1175/2008JTECHA1082.1.

830 Marquis, M. and P. Tans, 2008: Climate change - Carbon crucible. *Science*, **320**(5875): 460-
831 461.

832 Masarie, K. A., W. Peters, A. R. Jacobson, and P. P. Tans, 2014: ObsPack: a framework for
833 the preparation, delivery, and attribution of atmospheric greenhouse gas measurements,
834 *Earth Syst. Sci. Data*, **6**, 375–384, https://doi.org/10.5194/essd-6-375-2014.

835 McGill, M. J., L. Li, W. D. Hart, G. M. Heymsfield, D. L. Hlavka, P. E. Racette, L. Tian, M.
836 A. Vaughan, and D. M. Winker, 2004: Combined lidar-radar remote sensing: Initial
837 results from CRYSTAL-FACE, *J. Geophys. Res.: Atmos.*, **109**, D07203,
838 doi:10.1029/2003JD004030.

839 Michalak, A. M., R. B. Jackson, G. Marland, C. L. Sabine, and the Carbon Cycle Science
840 Working Group, 2011: A U.S. Carbon Cycle Science Plan, available at
841 http://carboncycle.joss.ucar.edu/sites/default/files/documents/USCarbonCycleSciencePla
842 n-2011.pdf.

843 Miles, N.L., S.J. Richardson, D.K. Martins, K.J. Davis, T. Lauvaux, B.J. Haupt, and S.K.
844 Miller, 2018: ACT-America: L2 In Situ CO2, CO, and CH4 Concentrations from Towers,
845 Eastern USA. ORNL DAAC, Oak Ridge, Tennessee, USA.
846 https://doi.org/10.3334/ORNLDAAC/1568.

847 Miles, N. L., S. J. Richardson, K. J. Davis, T. Lauvaux, A. E. Andrews, T. O. West, V.
848 Bandaru, and E. R. Crosson, 2012: Large amplitude spatial and temporal gradients in
849 atmospheric boundary layer CO2 mole fractions detected with a tower-based network in
850 the U.S. upper Midwest, *J. Geophys. Res.: Biogeosci.*, **117**, G01019,
851 doi:10.1029/2011JG001781.

852 Miller, S. M., and Coauthors, 2013: Anthropogenic emissions of methane in the United
853 States, *Proc. Natl. Acad. Sci. U.S.A.*, **110**(50), 20,018–20,022,
854 doi:10.1073/pnas.1314392110.

855 Montzka, S. A., and Coauthors, 2011: Non-CO2 greenhouse gases and climate change.
856 Nature, **476**(7358): 43-50.

857 Moore B. III, and Coauthors, 2018: The Potential of the Geostationary Carbon Cycle
858 Observatory (GeoCarb) to Provide Multi-scale Constraints on the Carbon Cycle in the
859 Americas. *Front. Environ. Sci.* **6**:109. doi: 10.3389/fenvs.2018.00109.

860 Myhre, G., D. and Coauthors, 2013: Anthropogenic and Natural Radiative Forcing. In:
861 *Climate Change 2013: The Physical Science Basis. Contribution of Working Group I to*
862 *the Fifth Assessment Report of the Intergovernmental Panel on Climate Change* [Stocker,
863 T.F., D. Qin, G.-K. Plattner, M. Tignor, S.K. Allen, J. Boschung, A. Nauels, Y. Xia, V.
864 Bex and P.M. Midgley (eds.)]. Cambridge University Press, Cambridge, United Kingdom
865 and New York, NY, USA.

866 Nalli, N.R., and Coauthors, 2020: Validation of Carbon Trace Gas Profile Retrievals from the
867 NOAA-Unique Combined Atmospheric Processing System for the Cross-Track Infrared
868 Sounder. *Remote Sens.* **12**, 3245.

869 Nisbet, E. G., E. J. Dlugokencky, and P. Bousquet, 2014: Methane on the rise—Again,
870 *Science*, **343**, 493–496, doi:10.1126/science.1247828.

871 O'Dell, C. W., and Coauthors, 2018: Improved retrievals of carbon dioxide from Orbiting
872 Carbon Observatory-2 with the version 8 ACOS algorithm, *Atmos. Meas. Tech.*, **11**,
873 6539–6576, https://doi.org/10.5194/amt- 11-6539-2018.

874 Ogle, S. M., and Coauthors, 2015: An approach for verifying biogenic greenhouse gas
875 emissions inventories with atmospheric CO_2 concentration data, *Environ. Res. Lett.,* **10**
876 034012 doi:10.1088/1748-9326/10/3/034012.

877 Pal, S., and Davis, K.J., 2020: ACT-America Field Campaign Catalogue. ORNL DAAC, Oak
878 Ridge, Tennessee, USA. https://actamerica.ornl.gov/campaigns.html.

879 Pal, S., and Coauthors, 2020a: Observations of greenhouse gas changes across summer
880 frontal boundaries in the eastern United States. *J. Geophys. Res.: Atmos.*, **125**,
881 e2019JD030526, https://doi.org/10.1029/2019JD030526.

882 Pal, S., K.J. Davis, R. Pauly, M. McGill, L. Campbell, K. Hoffman, A.M. Alejandro, M.
883 Rench, and H. Haas, 2020b: A brief description of the Cloud Physics Lidar-derived
884 atmospheric boundary layer top height data sets obtained using Wavelet transform
885 algorithm, ORNL DAAC, Oak Ridge, Tennessee, USA,
886 https://doi.org/10.3334/ORNLDAAC/1825.

887 Parazoo, N. C. and Coauthors, 2021: Covariation of airborne biogenic tracers (CO2, COS,
888 and CO) supports stronger than expected growing season photosynthetic uptake in the
889 southeastern US. In review, *AGU Advances*,
890 https://www.essoar.org/doi/abs/10.1002/essoar.10505574.1.

Parazoo, N. C., A. S. Denning, S. R. Kawa, K. D. Corbin, R. S. Lokupitiya, and I. T. Baker, 2008: Mechanisms for synoptic variations of atmospheric CO2 in North America, South America and Europe. *Atmos. Chem. Phys.*, **8**(23), 7239–7254. https://doi.org/10.5194/acp-8-7239-2008.

Parazoo, N. C., A. S. Denning, J. A. Berry, A. Wolf, D. A. Randall, S. R. Kawa, O. Pauluis, and S. C. Doney, 2011: Moist synoptic transport of CO2 along the mid-latitude storm track, *Geophys. Res. Lett.*, **38**(9), doi: 10.1029/2011GL047238.

Parazoo, N. C., A. S. Denning, S. R. Kawa, S. Pawson, and R. Lokupitiya, 2012: CO2 flux estimation errors associated with moist atmospheric processes, *Atmos. Chem. Phys.*, **12**(14), 6405–6416, doi:10.5194/acp-12- 6405-2012.

Peters, W., and Coauthors, 2007: An atmospheric perspective on North American carbon dioxide exchange: CarbonTracker. *Proc. Nat. Acad. Sci. U. S. A.,* **104**, 18,925–18,930. https://doi.org/10.1072/pnas.07089861074.

Peylin, P., and Coauthors, 2013: Global atmospheric carbon budget: results from an ensemble of atmospheric CO2 inversions, *Biogeosci.*, **10**, 6699-6720, doi:10.5194/bg-10-6699-2013.

Pickett-Heaps, C. A., and Coauthors, 2011: Atmospheric CO2 inversion validation using vertical profile measurements: Analysis of four independent inversion models, *J. Geophys. Res.: Atmos.*, **116**, D12305, doi:10.1029/2010JD014887.

Pisso, I., and Coauthors, 2019: The Lagrangian particle dispersion model FLEXPART version 10.4. *Geosci. Model Dev.*, **12**, 4955–4997, https://doi.org/10.5194/gmd-12-4955-2019.

913 Polonsky, I. N., D. M. O'Brien, J. B. Kumer, C. W. O'Dell, and the geoCARB Team, 2014:
914 Performance of a geostationary mission, geoCARB, to measure CO2, CH4 and CO
915 column-averaged concentrations. *Atmos. Meas. Tech.*, **7**(4), 959–981.
916 https://doi.org/10.5194/amt-7-959-2014.

917 Prather, M. J., C. M., Flynn, X. Zhu, S. D. Steenrod, S. A. Strode, A. M. Fiore, G. Correa, L.
918 T. Murray, and J.-F. Lamarque, 2018: How well can global chemistry models calculate
919 the reactivity of short-lived greenhouse gases in the remote troposphere, knowing the
920 chemical composition, *Atmos. Meas. Tech.*, **11**, 2653–2668, https://doi.org/10.5194/amt-
921 11-2653-2018.

922 Samaddar, A., S. Feng, T. Lauvaux, Z. R. Barkley, S. Pal and K. J. Davis, 2021: Carbon
923 dioxide distribution, origins, and transport along a frontal boundary during summer in
924 mid-latitudes. In review, *J. Geophys. Res.: Atmos.*,
925 https://www.essoar.org/doi/abs/10.1002/essoar.10503161.1.

926 Schuh, A., and Coauthors, 2019: Quantifying the Impact of Atmospheric Transport
927 Uncertainty on CO_2 Surface Flux Estimates, *Global Biogeochem. Cycles*, **33**, 484–500.
928 https://doi.org/10.1029/2018GB006086.

929 Schuh, A. E., and Coauthors, 2013. Evaluating atmospheric CO_2 inversions at multiple scales
930 over a highly-inventoried agricultural landscape. *Global Change Biol.*, **9**, 1424-1439, doi:
931 10.1111/gcb.12141.

932 Schuldt, K. and Coauthors, 2020: Multi-laboratory compilation of atmospheric carbon
933 dioxide data for the period 1957-2019; obspack_co2_1_GLOBALVIEWplus_v6.0_2020-
934 09-11; NOAA Earth System Research Laboratory, Global Monitoring Laboratory.
935 http://doi.org/10.25925/20200903.

936 Schwalm, C. R., and Coauthors, 2015: Toward “optimal” integration of terrestrial biosphere
937 models. *Geophys. Res. Lett.*, **42**(11), 4418–4428. https://doi.org/10.1002/2015GL064002.

938 Stein, A. F., R. R. Draxler, G. D. Rolph, B. J. B. Stunder, M. D. Cohen, and F. Ngan, 2015:
939 NOAA’s HYSPLIT Atmospheric Transport and Dispersion Modeling System. *Bull.*
940 *Amer. Meteor. Soc.* **96**(12), 2059–2077. https://doi.org/10.1175/BAMS-D-14-00110.1.

941 Stephens, B. B., and Coauthors, 2007: Weak northern and strong tropical land carbon uptake
942 from vertical profiles of atmospheric CO2. *Science*, **316**, 1732-1735,
943 doi:10.1126/science.1137004.

944 Stocker, T. F., and Coauthors, 2013: Climate Change 2013: The Physical Science Basis.
945 Contribution of Working Group I to the Fifth Assessment Report of the
946 Intergovernmental Panel on Climate Change, Cambridge University Press. Cambridge,
947 United Kingdom and New York, NY, USA.

948 Sweeney, C., and Coauthors, 2015: Seasonal climatology of CO2 across North America from
949 aircraft measurements in the NOAA/ESRL Global Greenhouse Gas Reference Network.
950 *J. Geophys. Res.: Atmos.*, **120**(10), 5155–5190. https://doi.org/10.1002/2014JD022591.

951 Tans, P P, I.Y. Fung, T. Takahashi, 1990: Observational constraints on the global
952 atmospheric CO_2 budget. *Science*, **247**, 1431-1438, doi:10.1126/science.247.4949.1431.

953 Thompson, R., and Coauthors, 2016: Top–down assessment of the Asian carbon budget since
954 the mid 1990s. *Nat. Commun.* **7**, 10724. https://doi.org/10.1038/ncomms10724

955 Turnbull, J. C., and Coauthors, 2015: Toward quantification and source sector identification
956 of fossil fuel CO_2 emissions from an urban area: Results from the INFLUX experiment.
957 *J. Geophys. Res. Atmos.*, **120**, doi:10.1002/2014JG022555.

958 Turner, A. J., C. Frankenberg, and E. A. Kort, 2019: Interpreting contemporary trends in
959 atmospheric methane. *Proc. Natl. Acad. Sci. U.S.A.*, **116**(8), 2805-2813.

960 USGCRP, 2018: Second State of the Carbon Cycle Report (SOCCR2): A Sustained
961 Assessment Report. [Cavallaro, N., G. Shrestha, R. Birdsey, M. A. Mayes, R. G. Najjar,
962 S. C. Reed, P. Romero-Lankao, and Z. Zhu (eds.)]. U.S. Global Change Research
963 Program, Washington, DC, USA, 878 pp., doi: 10.7930/SOCCR2.2018

964 Vermote, Eric; NOAA CDR Program, 2019: NOAA Climate Data Record (CDR) of AVHRR
965 Normalized Difference Vegetation Index (NDVI), Version 5. NOAA National Centers for
966 Environmental Information. https://doi.org/10.7289/V5ZG6QH9. Accessed 6 December,
967 2020.

968 Wang, Q., S. Crowell, and S. Pal., 2021: Atmospheric variations in column integrated CO2
969 on synoptic and seasonal time scale over the U.S., In review, *J. Geophys. Res.: Atmos.*,
970 https://www.essoar.org/doi/pdf/10.1002/essoar.10505706.1.

971 Wei, Y, and Coauthors, 2021: Atmospheric Carbon and Transport – America (ACT-America)
972 Datasets: Description, Management, and Delivery. In review, *Earth Space Sci.*,
973 https://www.essoar.org/doi/pdf/10.1002/essoar.10505692.1.

974 Weibring, P., and Coauthors, 2020: Autonomous airborne mid-infrared spectrometer for
975 high-precision measurements of ethane during the NASA ACT-America studies, *Atmos.*
976 *Meas. Tech.*, **13**, 6095–6112, https://doi.org/10.5194/amt-13-6095-2020.

977 Wesloh, D., T. Lauvaux, and K. J. Davis, 2020: Development of a mesoscale inversion
978 system for estimating continental-scale CO2 fluxes. *J. Adv. Model. Earth Sys.*,**12**,
979 e2019MS001818. https://doi.org/10.1029/2019MS001818.

WMO, 2018: 19th WMO/IAEA Meeting on Carbon Dioxide, Other Greenhouse Gases and Related Measurement Techniques (GGMT-2017). GAW Report No. 242. Edited by Andrew Crotwell and Martin Steinbacher.

Wunch, D., and Coauthors, 2017: Comparisons of the Orbiting Carbon Observatory-2 (OCO-2) *X*CO2 measurements with TCCON, *Atmos. Meas. Tech.*, **10**, 2209–2238, https://doi.org/10.5194/amt-10-2209-2017.

Wunch, D., and Coauthors, 2011: The Total Carbon Column Observing Network. *Philos. Trans. R. Soc. A*, **369**(1943), 2087–2112. https://doi.org/10.1098/rsta.2010.0240.

Yin, Y., and Coauthors, 2020: Cropland carbon uptake delayed and reduced by 2019 Midwest floods. *AGU Adv.*, **1**, e2019AV000140. https://doi.org/10.1029/2019AV000140

Yokota, T., Y. Yoshida, N. Eguchi, Y. Ota, T. Tanaka, H. Watanabe, and S. Maksyutov, 2009: Global Concentrations of CO_2 and CH_4 Retrieved from GOSAT: First Preliminary Results, *SOLA*, **5**, 160–163.

Zhou, Y., and Coauthors, 2020: A multiyear gridded data ensemble of surface biogenic carbon fluxes for North America: Evaluation and analysis of results. *J. Geophys. Res.: Biogeosci.*, **125**, e2019JG005314. https://doi.org/10.1029/2019JG005314.

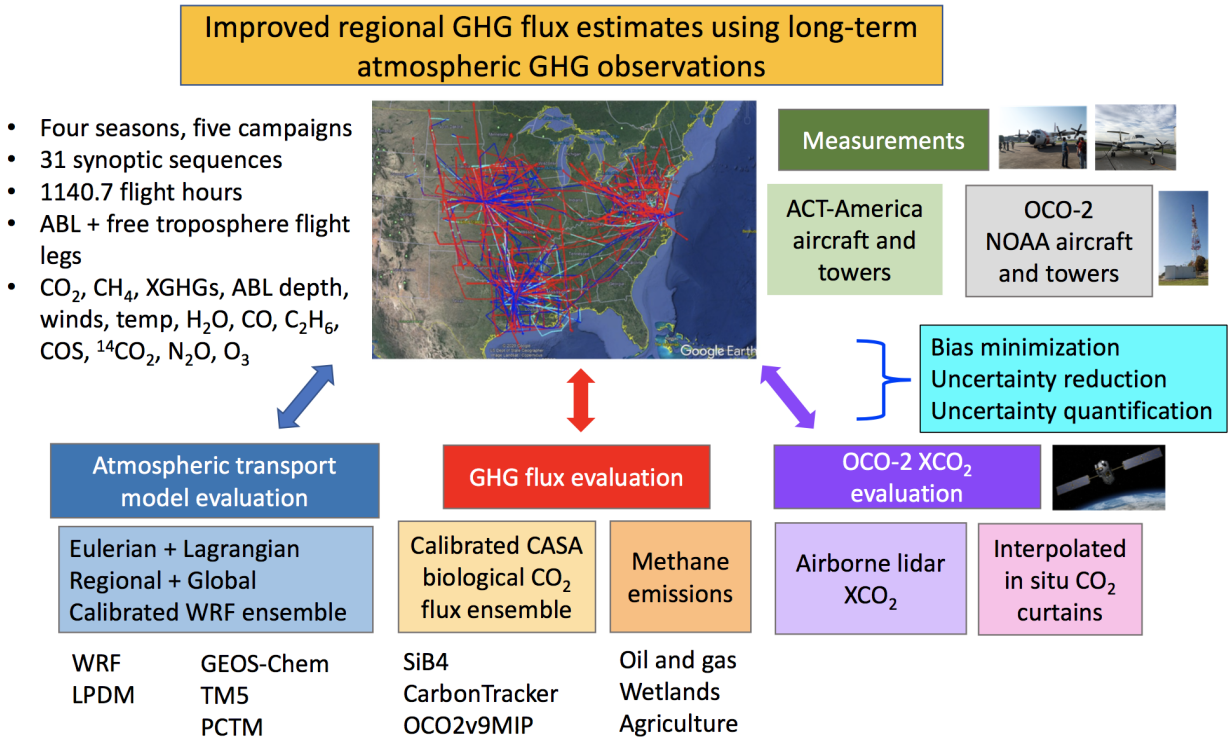

997

998 **Figure 1**. ACT-America measurements complement long-term in situ and remote sensing
999 GHG observations by providing the first detailed measurements of the GHG structure of 31
1000 synoptic weather systems that passed through the central and eastern United States, a region
1001 of strong, seasonally-varying GHG fluxes and vigorous mixing by mid-latitude cyclones. The
1002 GHG and meteorological observations are complemented with ensembles of atmospheric and
1003 ecosystem models, and measurements of trace gases, that aid in disaggregating GHG sources.
1004 Improved GHG flux estimates are pursued by minimizing biases and random errors, and
1005 quantifying the remaining uncertainty in atmospheric transport simulations, GHG flux
1006 models, and OCO-2 XCO_2 observations. These improved components can be incorporated
1007 into atmospheric inversion systems. ACT-America observations are also used as independent
1008 data to evaluate existing atmospheric inversion systems. The joint observations of greenhouse
1009 gases, associated trace gases and atmospheric transport variables help to detangle the difficult
1010 issue of combined atmospheric transport and C flux biases that are present in all atmospheric

1011 inversion studies. The central image overlays all ACT-America flight tracks. Images show
1012 the NASA C-130 and B-200 aircraft, an instrumented communications tower, and a rendering
1013 of the OCO-2 satellite platform.

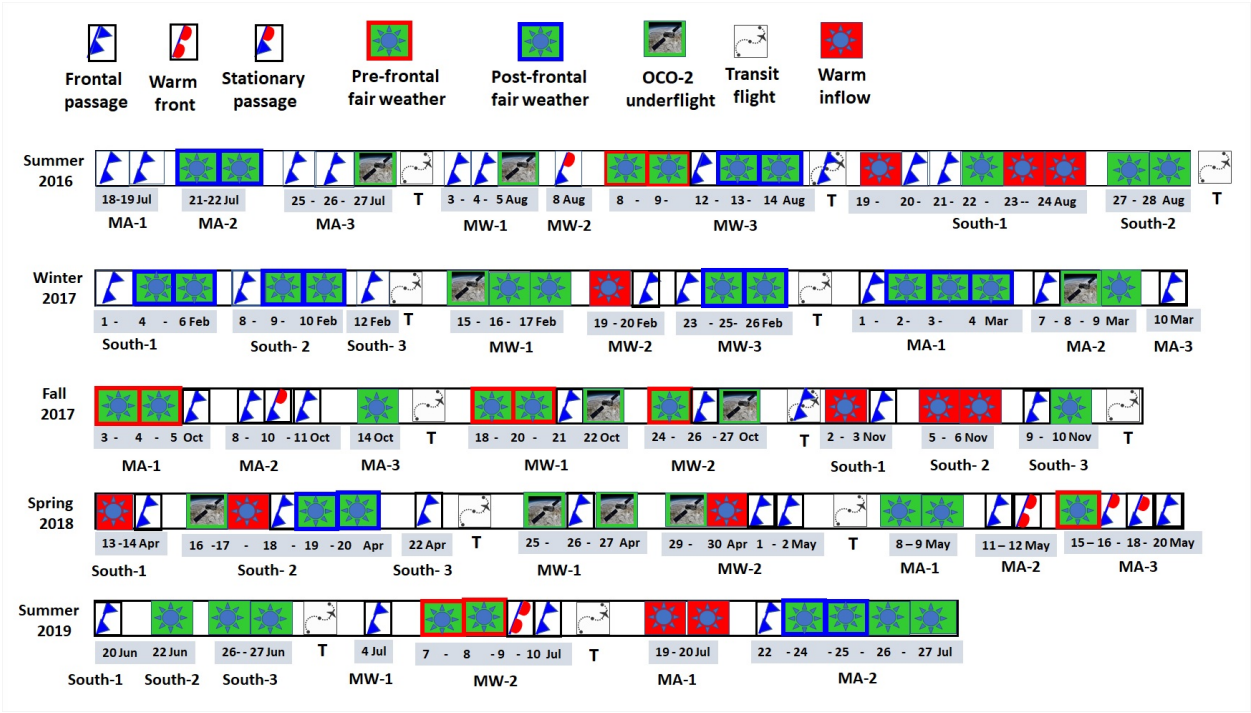

Figure 2. Pictorial representation of the sequence of ACT-America research flights. Some hybrid flights only have their primary purpose indicated. MA and MW refer to the MidAtlantic and MidWest regions, respectively, the number refers to the synoptic sequence within a season and region, and T refers to a transit flight. Details about the flight tracks, scientific objectives, weather conditions and quick data visualizations are available in the ACT-America campaign catalogue (Pal and Davis, 2020; https://actamerica.ornl.gov/campaigns.html).

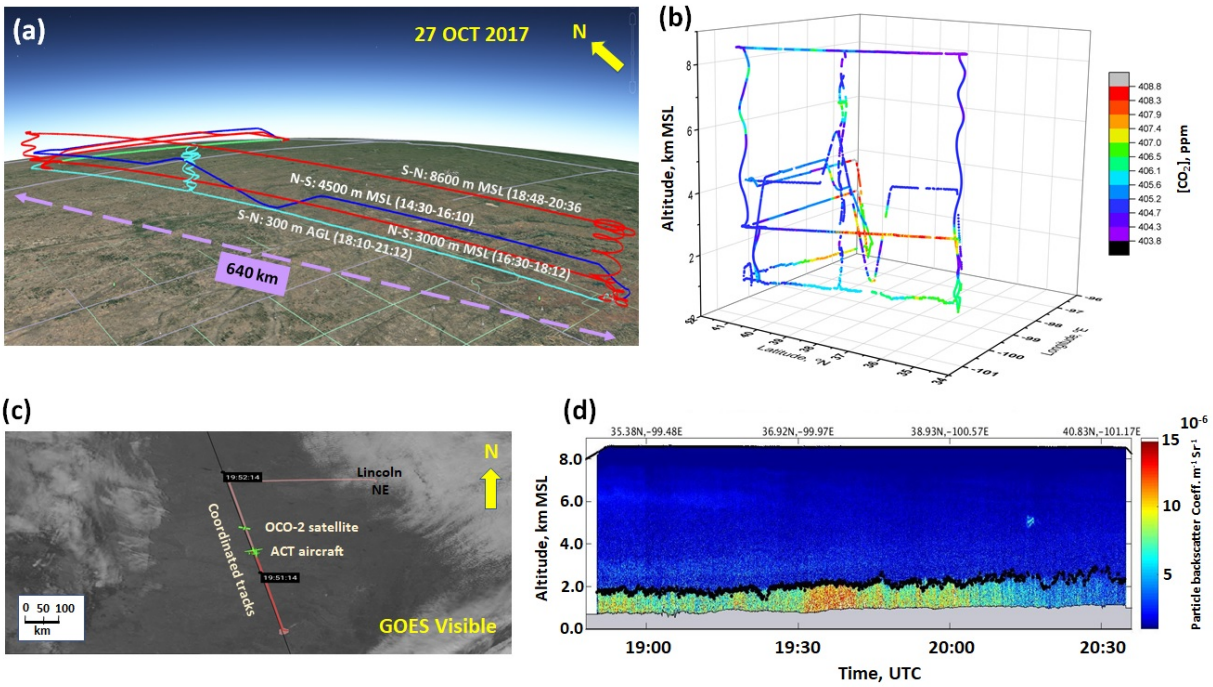

1022

1023 **Figure 3:** OCO-2 under flight from 27 October, 2017. (a) The aircraft flew at multiple
1024 altitudes to measure (b) in situ CO_2 along the OCO-2 sampling swath. The C-130 flew at its
1025 maximum altitude on one pass to measure partial column XCO_2 (Campbell et al, 2020) with
1026 the Multifunctional Fiber Laser Lidar (MFLL). The flight was coordinated so that, (c) at the
1027 midpoint in time of the flight pattern, the C-130 was at maximum altitude directly overflying
1028 the B-200, which was performing an in situ spiral from 300 m AGL up to the altitude of the
1029 C-130 overpass, when the OCO-2 satellite overflew both aircraft. (d) The Cloud Physics
1030 Lidar (CPL) mapped out backscatter (color scale) and a wavelet algorithm was used to
1031 retrieve ABL depth (solid black line) along the flight track.

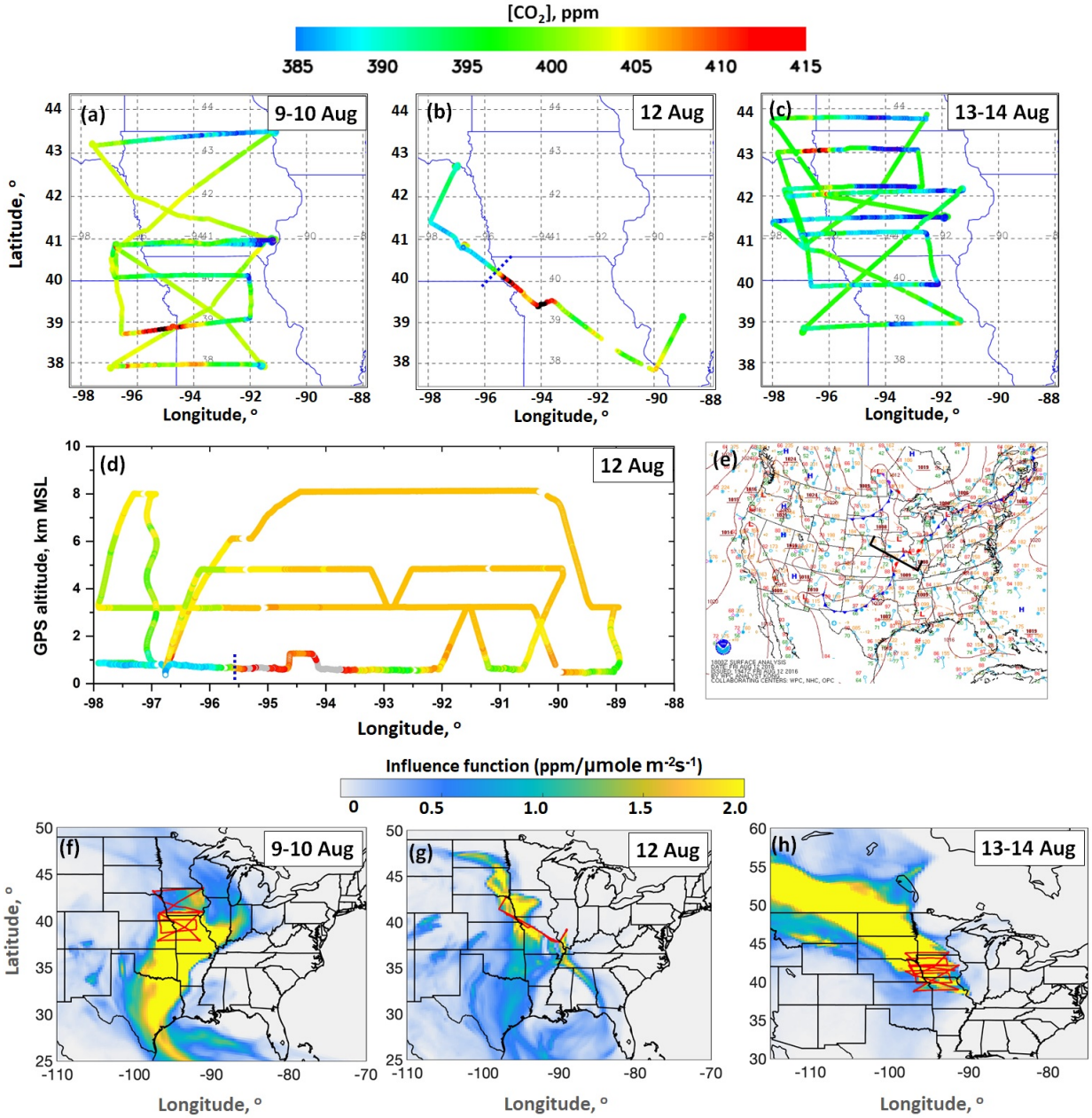

1032

1033 **Figure 4.** Illustration of a MidWest synoptic sequence from the Summer, 2016 flight

1034 campaign. (a-c) Flight tracks for 9 - 14 August, 2016 showing in situ CO_2 measured along

1035 the tracks (only ABL CO_2 is shown on 12 August when multiple tracks were stacked in the

1036 vertical). Fair weather portions include ABL (east-west legs) and lower free tropospheric

1037 (diagonal and north-south) flight legs arrayed in quasi-Lagrangian 2-day sequences. (d)

1038 Latitude vs. altitude CO_2 mole fractions during the frontal crossing on 12 August. The

1039 approximate surface frontal position is marked with the dotted black line. (e) The surface

weather map for 18 UTC on 12 August (courtesy of the NOAA Weather Prediction Center, http://www.wpc.ncep.noaa.gov) shows synoptic conditions with the flight track position overlaid. (f-h) The associated upwind influence functions for the ABL portions of each flight.

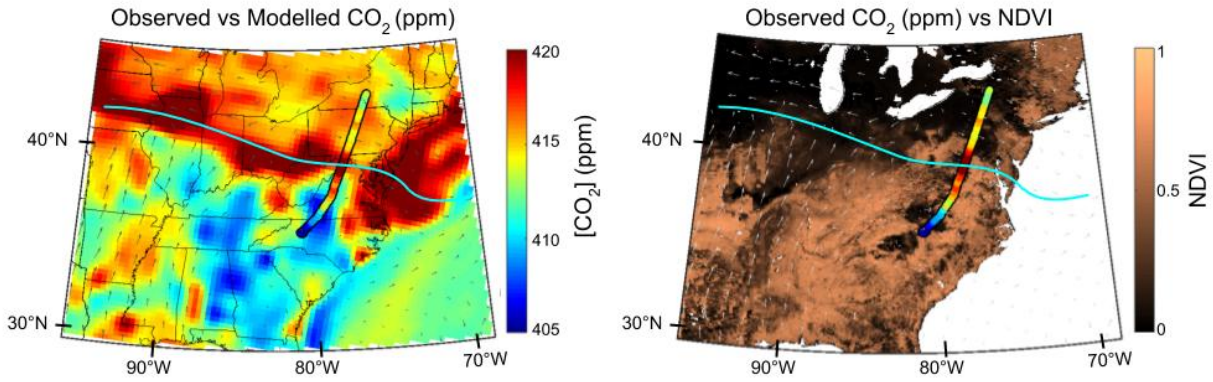

1043

1044 **Figure 5**. (Left) Observed vs simulated ABL CO_2 for the flight of 11 May, 2018. Simulated
1045 CO_2 mole fractions and wind barbs are plotted at 500 m AGL at 18Z; flight altitude was
1046 roughly 300 m AGL and took place between 16-19Z. The simulation is from the ACT-
1047 America WRF baseline run, with CarbonTracker surface fluxes and lateral boundary
1048 conditions (Feng et al, 2020). (Right) Observed ABL CO_2 mole fraction and normalized
1049 difference vegetation index (NDVI) during the day of the flight (Vermote, 2019). The teal
1050 line marks the approximate location of a stationary front that was present at that time.

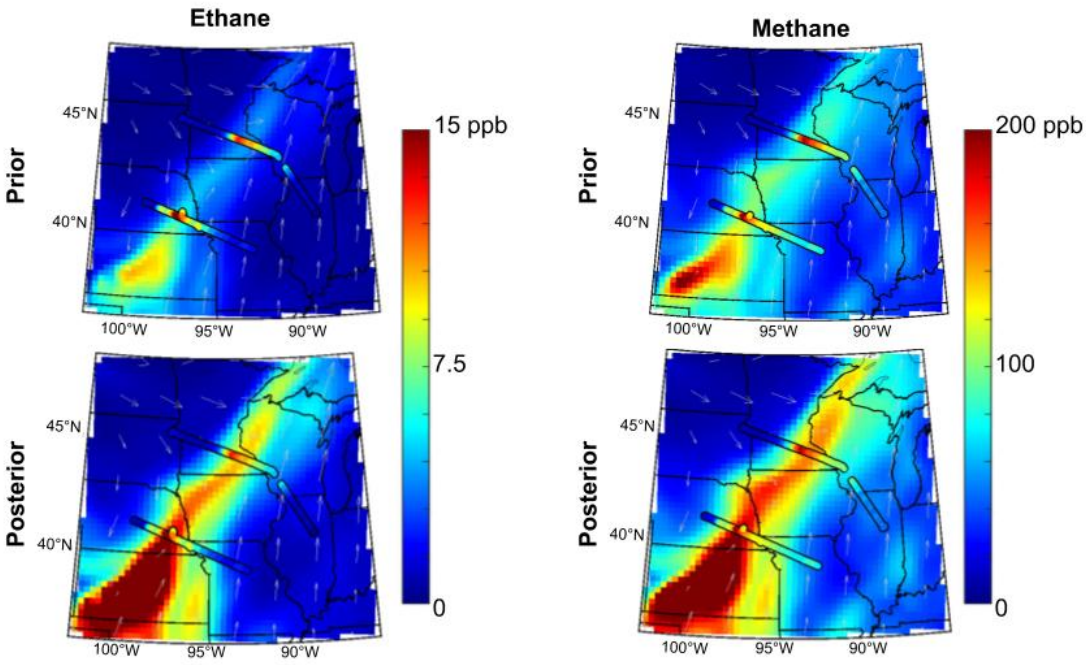

Figure 6. Example of a dual-tracer optimization used to solve for methane emissions on 18 October, 2017. (top-left) Observed vs. simulated ABL ethane mole fraction enhancements relative to a background based on oil and gas sources from the EPA 2012 Gridded Methane Inventory (Massaakers et al, 2016) and an assumed average ethane:methane gas composition of 0.10 (a reasonable overall estimate for US oil and gas production). (bottom-left) Observed vs. simulated ABL ethane enhancements achieved by multiplying oil and gas emissions by a factor of 2.5. (top-right) Observed vs. simulated ABL methane enhancements based on the same inventory. (bottom-right) Observed vs. simulated ABL methane enhancements achieved by multiplying oil and gas emissions by a factor of 2.5. In all panels, simulated mole fractions (Feng et al, 2020) are from 500 m AGL at 19 UT. Aircraft observations are from approximately 300 m AGL and were collected between 17-21 UT. A surface cold front parallels the northwest portion of the region of enhanced methane and ethane. The enhanced mole fractions are in the warm sector flowing to the north and east. The ethane observations enable source disaggregation (animal agriculture vs. oil and gas production) using the ethane/methane emissions ratios. Methods follow Barkley et al. (2019a).

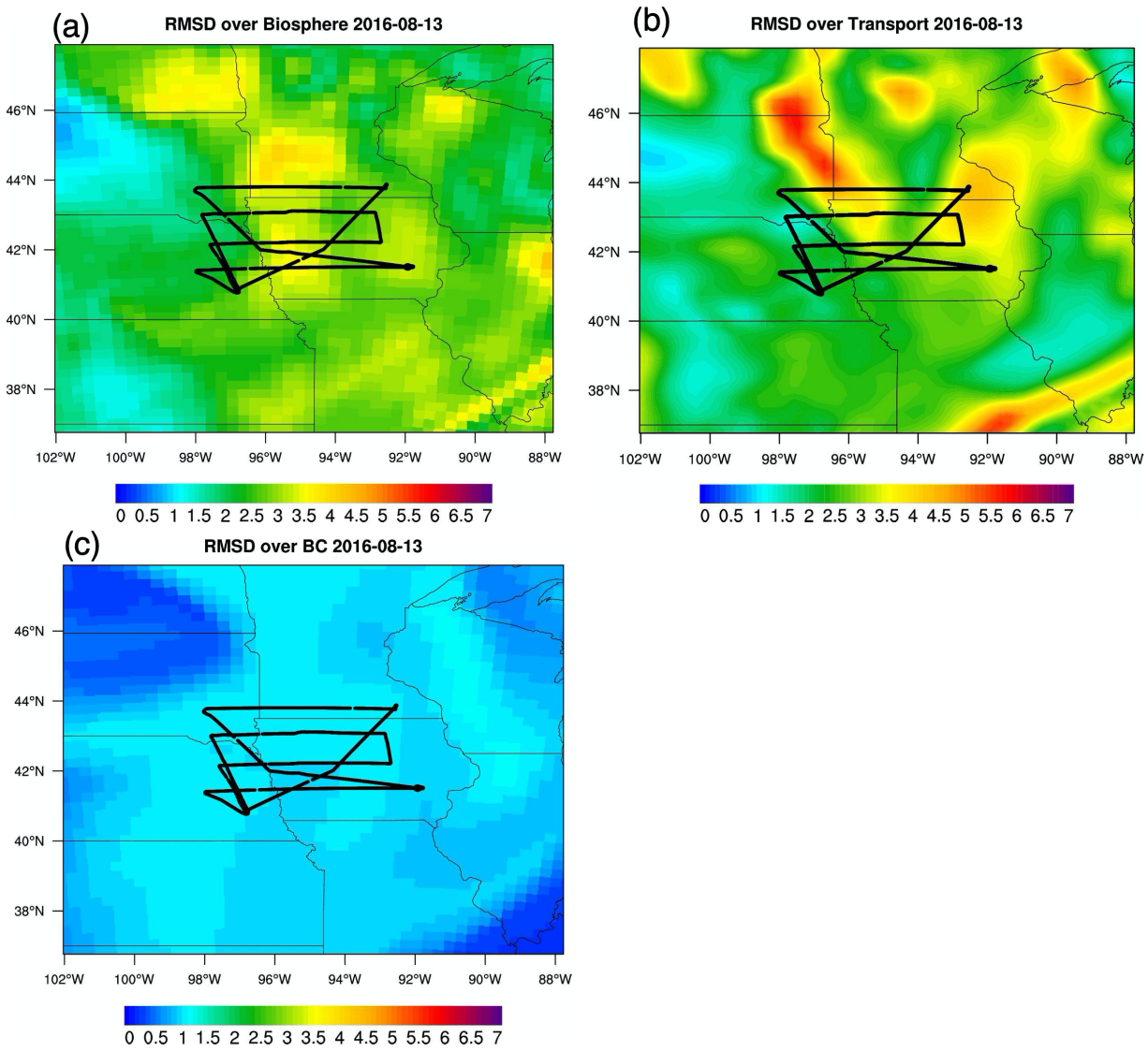

1067

1068 **Figure 7.** Root mean square deviation in ABL CO_2 mole fractions (500 m AGL) across

1069 components of the multi-component ensemble simulation system described by Feng et al.

1070 (2021) at 19 UT on 13 August, 2016, one of the fair weather flight days shown in Figure 4,

1071 including: (a) RMSD across the CASA biological flux ensemble members, (b) RMSD across

1072 the atmospheric transport ensemble members, and (c) RMSD across the continental boundary

1073 condition ensemble members. In each case, all other components of the ensemble are held

1074 constant. The black lines show the aircraft flight patterns on this day. Feng et al. (2019b)

1075 demonstrated the calibration of this multi-component ensemble, but with a different

biological CO_2 flux ensemble. The CASA ensemble may underestimate the true flux uncertainty (Feng et al., 2021).